© 2021. Published by The Company of Biologists Ltd | Development (2021) 148, dev188656. doi:10.1242/dev.188656

TECHNIQUES AND RESOURCES

RESEARCH ARTICLE

Embryonic development in the acoel *Hofstenia miamia*

Julian O. Kimura, Lorenzo Ricci and Mansi Srivastava*

ABSTRACT

Acoels are marine worms that belong to the phylum Xenacoelomorpha, a deep-diverging bilaterian lineage. This makes acoels an attractive system for studying the evolution of major bilaterian traits. Thus far, acoel development has not been described in detail at the morphological and transcriptomic levels in a species in which functional genetic studies are possible. We present a set of developmental landmarks for embryogenesis in the highly regenerative acoel *Hofstenia miamia*. We generated a developmental staging atlas from zygote to hatched worm based on gross morphology, with accompanying bulk transcriptome data. *Hofstenia* embryos undergo a stereotyped cleavage program known as duet cleavage, which results in two large vegetal pole 'macromeres' and numerous small animal pole 'micromeres'. These macromeres become internalized as micromere progeny proliferate and move vegetally. We also noted a second, previously undescribed, cell-internalization event at the animal pole, following which we detected major body axes and tissues corresponding to all three germ layers. Our work on *Hofstenia* embryos provides a resource for mechanistic investigations of acoel development, which will yield insights into the evolution of bilaterian development and regeneration.

KEY WORDS: Acoel, Embryogenesis, Developmental transcriptome, Duet cleavage

INTRODUCTION

Acoel worms are a group of marine invertebrates that have garnered attention in the fields of evolutionary and regenerative biology because of their phylogenetic placement and the extensive regenerative capacity of some species (Bourlat and Hejnol, 2009; Gehrke et al., 2019; Gehrke and Srivastava, 2016; Hejnol and Pang, 2016; Srivastava et al., 2014). Based on morphological characteristics and striking similarities in cell cleavage patterns during early embryogenesis, acoels were thought to belong to the phylum Platyhelminthes (Ax and Dörjes, 1966; Ax and Jeffries, 1987; Boyer et al., 1996; Boyer and Jonathan, 1998; Bresslau, 1909; Costello and Henley, 1976; Henry and Martindale, 1999; Hyman, 1951; Peterson and Eernisse, 2001; Smith et al., 1986). Members of the phylum Platyhelminthes develop using an ancestral cleavage program called spiral cleavage (four large vegetal blastomeres producing smaller cells toward the animal pole), whereas acoel worms undergo duet cleavage (two large vegetal blastomeres producing smaller cells toward the animal pole) (Apelt, 1969; Boyer, 1971; Bresslau, 1909; Henry et al., 2000; Maslakova et al., 2004; Nielsen, 1995). Given that acoels were nested within a group with an ancestral spiral cleavage program, it was hypothesized that duet cleavage was a derived form of spiral cleavage. However, recent molecular phylogenetic analyses have revealed that acoels belong to the major animal clade Xenacoelomorpha, which represents either the sister group to all other bilaterians (Nephrozoa) or to a deuterostome lineage (Ambulacraria) (Fig. 1A) (Hejnol et al., 2009; Jondelius et al., 2011; Kapli et al., 2021; Kapli and Telford, 2020; Marlétaz et al., 2019; Mwinyi et al., 2010; Philippe et al., 2007, 2011, 2019; Ruiz-Trillo et al., 1999, 2002, 2004; Ruiz-Trillo and Paps, 2016; Sempere et al., 2007; Telford et al., 2003). Both of these phylogenetic positions for Xenacoelomorpha make acoels highly informative for understanding the evolution of bilaterian traits. Moreover, in either scenario, xenacoelomorphs are distantly related to platyhelminths and to other animals that undergo spiral cleavage. This raises the possibility that the cleavage program in acoels represents an independently evolved, yet understudied, mode of development. Therefore, in addition to providing insights into the evolution of bilateral symmetry, mesoderm and a centralized nervous system (Bourlat and Hejnol, 2009; Hejnol and Pang, 2016), studies of acoel embryogenesis could reveal new mechanisms of development.

All acoel species studied thus far were found to undergo duet cleavage (Apelt, 1969; Boyer, 1971; Bresslau, 1909; Henry et al., 2000), which features embryos with two large blastomeres (macromeres) on the vegetal pole that divide asymmetrically to produce several smaller blastomeres (micromeres) on the animal pole (Fig. S1A). The vegetal macromeres are then internalized as the micromeres continue to proliferate and move towards the vegetal pole. Fate-mapping experiments in the species *Neochildia fusca* revealed that micromeres give rise to ectodermal fates, whereas macromeres labeled immediately prior to internalization give rise to the endomesoderm (Henry et al., 2000). Furthermore, the expression of the gene *brachyury*, which is associated with gastrulation in many different animal lineages, was detected at the site of macromere internalization in the species *Convolutriloba longifissura* (Arendt et al., 2001; Hejnol and Martindale, 2008a; Technau, 2001). Although these results are from two separate species, given the conservation of the duet cleavage program, it was hypothesized that the process of macromere internalization represented gastrulation in acoels. Insights into acoel development, such as staging, gene expression and myogenesis, are available from different species (Hejnol and Martindale, 2008a,b; Ladurner and Rieger, 2000; Perea-Atienza et al., 2018; Ramachandra et al., 2002; Semmler et al., 2008). However, systematic studies of embryogenesis in one system, particularly a genetically tractable research organism, are needed to obtain mechanistic insights into acoel development and the evolution of bilaterian traits.

Here, we present a morphological and molecular characterization of embryogenesis in the acoel worm *Hofstenia miamia*, a new research organism for studying acoel development and regeneration (Fig. 1B,C) (Gehrke et al., 2019; Srivastava et al., 2014). *Hofstenia* is a genetically tractable model system with molecular resources including a high-quality genome and transcriptome

Department of Organismic and Evolutionary Biology, Museum of Comparative Zoology, Harvard University, Cambridge, MA 02138, USA.

*Author for correspondence (mansi@oeb.harvard.edu)

M.S., 0000-0002-2126-8634

Handling Editor: James Briscoe
Received 18 January 2021; Accepted 20 May 2021

Development (2021) 148, dev188656. doi:10.1242/dev.188656

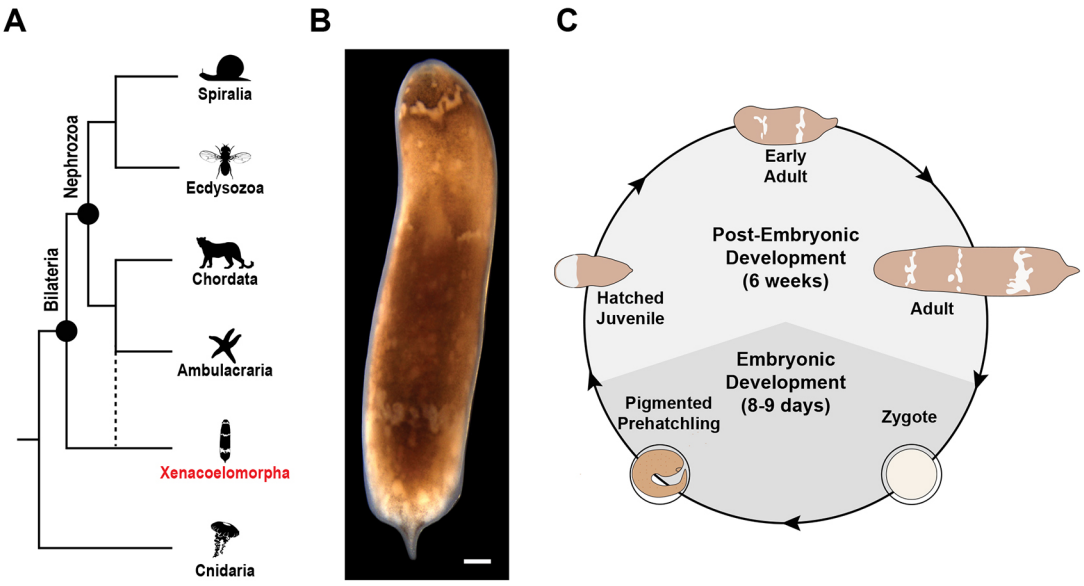

Fig. 1. *Hofstenia miamia* as an acoel model for studies of embryogenesis. (A) Acoels belong to the phylum Xenacoelomorpha (red), which is sister either to all other bilaterians (nephrozoans) or to ambulacrarians. Animal silhouettes were obtained from phylopic (phylopic.org). The image depicting ambulacrarians was created by Mali'o Kodis, photograph by 'Wildcat Dunny' (https://www.flickr.com/photos/wildcat_dunny/) and is reproduced under a Creative Commons Attribution 3.0 Unported license. (B) Brightfield image of an adult *H. miamia*. (C) *H. miamia* life cycle, based on a schematic developed by Dr Yi Jyun Luo (University of Oxford, UK). Light gray represents post-embryonic development, whereas dark gray represents embryonic development. Sexually mature adult worms lay fertilized zygotes that hatch into a juvenile worm in 8 to 9 days. The hatched juvenile worm then undergoes post-embryonic development into a sexually mature adult. Scale bar: 100 µm in B.

(Gehrke et al., 2019; Srivastava et al., 2014). *Hofstenia* can be cultured easily in the lab and produces plentiful, accessible embryos that are amenable to experimental manipulation (Fig. S1B,C). Furthermore, the ability of *Hofstenia* to undergo whole-body regeneration using putatively pluripotent stem cells provides a unique opportunity to study how a highly regenerative animal undergoes development. The established repertoire of tools for studying regeneration in *Hofstenia*, such as systemic RNA interference (RNAi), makes it an excellent model for studying acoel development. We staged *Hofstenia* embryos from zygote to hatching over a 9-day period, characterized their duet cleavage pattern, identified two major cell-internalization events, generated transcriptome data in bulk for each stage and determined the timing for the detection of body axes and differentiated tissues. This work serves as a foundation for future mechanistic studies of acoel embryogenesis and regeneration, which could ultimately provide insights into the evolution of bilaterian traits and regeneration.

RESULTS

A developmental atlas for *Hofstenia miamia*

We generated a developmental atlas based on gross morphology, phalloidin staining and nuclear labeling for *H. miamia* (Fig. 2A,B, Fig. 3A,B; Movies 1, 2). Hermaphroditic adults produce embryos that develop directly into juvenile worms, which hatch 8 to 9 days later (Fig. 1C). Embryos are laid in clutches as spherical, fertilized zygotes (0 h post laying; hpl), ∼300 µm in diameter (Fig. 2A; Fig. S1D; Movies 1, 2). The zygotes are opaque and each is enveloped in a clear egg shell upon laying (Fig. S1D). Developmental timing is denoted in hpl at 23°C.

Early-cleavage stage (0-22 hpl)

Much like previously studied acoels, *Hofstenia* embryos undergo a stereotyped, duet cleavage pattern during early development. The early-cleavage stage begins with the initiation of cell division and ends with a cell movement event that results in the internalization of vegetal cells (Fig. 2A; Fig. S2A; Movies 1, 2). The first cleavage is symmetric and produces two blastomeres, which we refer to as A and B (7 hpl), following the convention in previously published descriptions of acoel embryogenesis (Boyer, 1971; Bresslau, 1909; Henry et al., 2000). During the second cleavage, blastomeres A and B divide synchronously and asymmetrically, producing smaller progeny towards the animal pole laeotropically (i.e. in a counter-clockwise orientation when viewed from the animal pole). This results in a four-cell embryo in which smaller cells, micromeres 1a and 1b, are generated at a 45° angle to the animal-vegetal (AV) axis. The larger cells on the vegetal pole are now referred to as macromeres 1A and 1B. Micromeres 1a and 1b sit at the cell junction of macromeres 1A and 1B.

Next, micromeres and macromeres enter a phase of sequential division in which micromeres cleave first, synchronously relative to each other, followed by asymmetric, synchronous cleavage of macromeres. Micromeres 1a and 1b cleave laeotropically and asymmetrically at a 45° angle relative to the AV axis, producing two progeny each: $1a^1$, $1a^2$ and $1b^1$, $1b^2$, respectively. The $1a^1$ and $1b^1$ blastomeres are smaller than $1a^2$ and $1b^2$. This results in an embryo with six cells: four micromeres and two macromeres. The 1A and 1B macromeres then cleave laeotropically and asymmetrically to produce micromeres 2a and 2b towards the animal pole and macromeres 2A and 2B on the vegetal pole, resulting in an eight-cell embryo.

The $1a^1$, $1b^1$, $1a^2$ and $1b^2$ cells then cleave symmetrically and synchronously. The $1a^2$ and $1b^2$ cells cleave at a 45° angle to the AV axis, whereas $1a^1$ and $1b^1$ cleave perpendicular to the AV axis. These cleavages produce a 12-cell embryo. Next, a 14-cell embryo forms, with the 2a and 2b cells cleaving symmetrically along the AV axis. The macromeres then undergo an additional laeotropic, asymmetric division to produce the 3a and 3b micromeres and 3A and 3B macromeres, generating a 16-cell embryo. After the 16-cell stage, the 'cap' of micromeres at the animal pole appears to move towards the vegetal pole as further cell divisions occur (17-22 hpl), enveloping

Development (2021) 148, dev188656. doi:10.1242/dev.188656

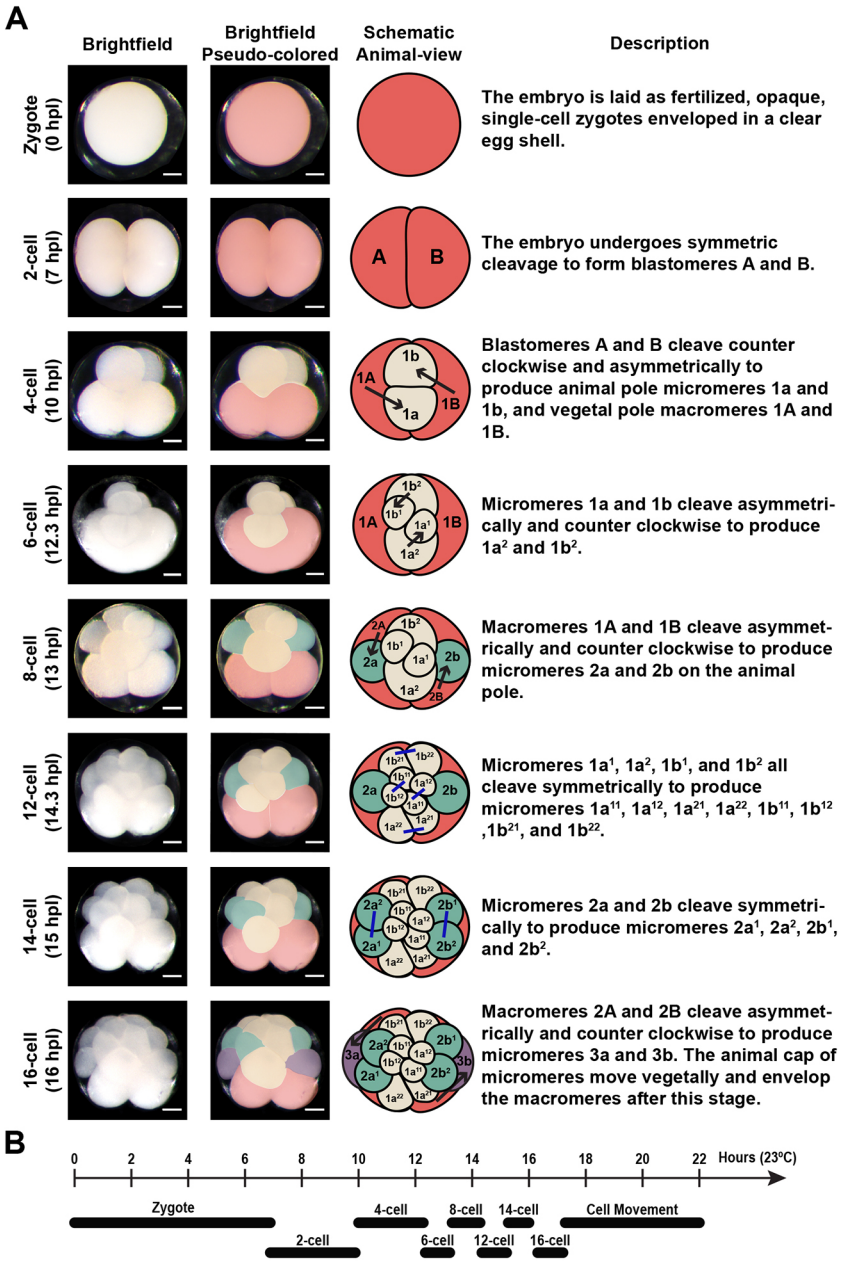

Fig. 2. The acoel worm *Hofstenia miamia* undergoes a stereotyped, duet cleavage program. (A) From left to right: representative brightfield images of live *Hofstenia* embryos showing early cleavages; representative brightfield images pseudo-colored to show distinct blastomeres and their daughter cells; animal-view schematic of the cleavage order, with arrows signifying asymmetric cleavage and blue lines signifying symmetric cleavage; defining characteristics of each developmental stage. Macromeres are shown in red; yellow indicates the first set of micromeres and their progeny; green indicates the second set of micromeres and their progeny; purple represents the third set of micromeres. (B) Schematic timeline of *Hofstenia* early cleavage. Scale bars: 100 µm in A.

the larger macromeres (Movies 1, 2). This envelopment of the macromeres represents the first instance of cell internalization during *Hofstenia* development. Individual cleavages that occur after the 16-cell stage could not be discerned under a dissecting microscope.

Gastrula stage (23-40 hpl)

Once the large macromeres are completely enveloped, the embryo becomes a spherical cluster of cells with macromeres occupying the interior (Fig. 3A). Given that this process of macromere internalization is conserved among acoels and is considered to represent gastrulation, we refer to this as the gastrula stage (Henry et al., 2000). This ‘ball’ of cells is solid, with no blastocoel-like cavity detectable (Fig. S3A). The cells at the surface of the embryo display a rough, uneven texture. The majority of nuclei at this stage have a distinct shape, with diffuse chromosomes appearing to be organized around a point, resembling a flower-like shape, which we refer to as a ‘rosette’ (Fig. S3B). We found that nuclei undergoing division do not have rosette-shaped nuclei and, instead, have condensed chromosomes, some appearing to be segregating to opposite poles, suggestive of anaphase.

Dimple stage (41-55 hpl)

As cells continue to divide, time-lapse microscopy revealed that a ‘dimple’ forms on one side of the embryo, where cells appear to be internalized (Fig. 3A; Movie 1). Therefore, we refer to embryos during this time as the dimple stage. This represents a second, previously undescribed cell-internalization event during embryogenesis in an acoel. During the dimple stage, a ring of concentrated actin forms at the site of the dimple (Fig. 3A; Fig. S2B). This ring of actin progressively becomes constricted as development continues during this stage and as the dimple becomes smaller. Instead of the rosette-shaped nuclei that were detected during the gastrula stage, many dimple-stage nuclei resemble a ‘donut’, forming a ring with an empty space at its center (Fig. S3B).

Development (2021) 148, dev188656. doi:10.1242/dev.188656

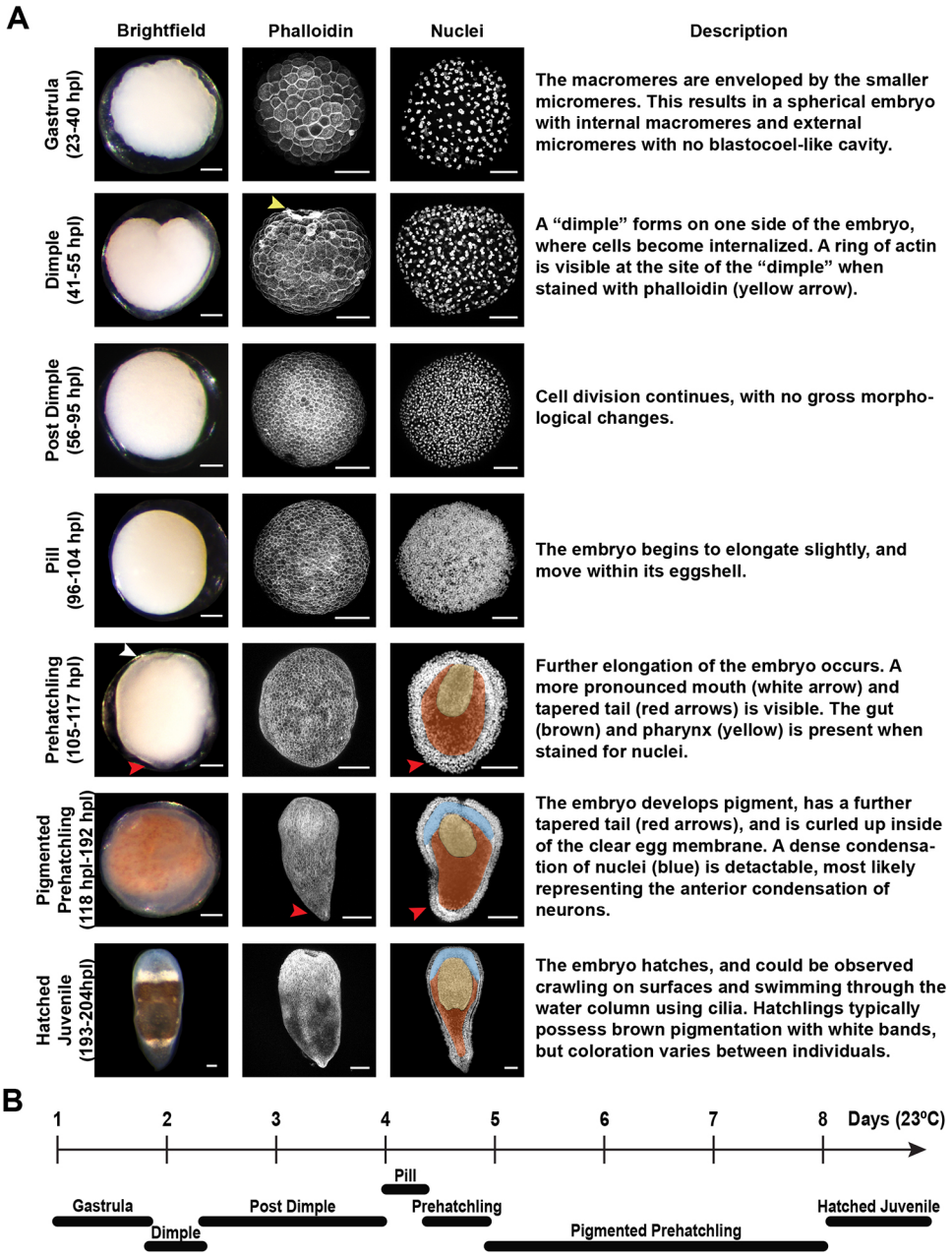

Fig. 3. Developmental atlas of later stages of *Hofstenia miamia* embryogenesis. (A) From left to right: representative brightfield images of live *Hofstenia* embryos showing later stages; phalloidin and nuclear staining of each corresponding developmental stage; and the defining characteristics of each developmental stage. Yellow arrowhead indicates the ring of actin at the site of the dimple; white arrowhead indicates the opening of the mouth; red arrowheads show the tapered posterior; yellow shading indicates the tube-like distribution of nuclei connected to the mouth, signifying the presence of a pharynx; brown shading represents the region of sparse nuclei, signifying the presence of a gut; blue shading indicates the region of densely packed nuclei on the anterior, signifying the presence of the anterior condensation of neurons. (B) Schematic timeline of later *Hofstenia* developmental stages. Scale bars: 100 µm.

Post-dimple stage (56-95 hpl)

The dimple becomes smaller in size and the embryo acquires a smooth, spherical shape during the post-dimple stage (Fig. 3A). Cells are now small enough to give the surface of the embryo an even, smooth texture. During this stage, although cell divisions continue, the embryo does not exhibit gross morphological changes. We did not detect rosette- or ring-shaped nuclei at this stage; instead, nuclei adopted a more spherical shape (Fig. S3B).

Pill stage (96-104 hpl)

As cell division continues, the embryo becomes less spherical, adopting an oval shape, and can be observed spinning within its egg shell during the pill stage (Fig. 3A; Movie 1). However, no body wall movement could be observed. Labeling of the cell membranes revealed the presence of cilia on the outer cells of the embryo, suggesting that the movement observed during this stage was the result of ciliary action (Fig. S4).

Prehatchling stage (105-117 hpl)

The embryo continues to elongate and the anterior-posterior (AP) axis is clearly identifiable by the presence of a mouth (anterior) and a tapered tail (posterior) during the prehatchling stage (Fig. 3A). The embryo moves its body wall within its egg shell, suggesting the use of muscle (Movie 1). A region with sparsely distributed nuclei is observed at the center of the embryo, which suggests the presence of the gut. A tube-like pattern of nuclei at the anterior of the embryo is also visible, which signifies the presence of a pharynx.

Pigmented-prehatchling stage (118-192 hpl)

During the pigmented-prehatchling stage, the embryo continues to elongate its body axis and the posterior becomes tapered further, resembling a hatched juvenile worm that is curled within the egg shell (Fig. 3A). Brown-and-white pigment granules form throughout the embryo. The embryo also moves vigorously within its egg shell. Furthermore, the space between the embryo and the

Development (2021) 148, dev188656. doi:10.1242/dev.188656

egg shell diminishes and the embryo can be seen pushed up against the internal wall of the shell immediately prior to hatching. The anterior region of the embryo is densely populated by nuclei at this stage, which corresponds to the anterior condensation of neurons that are present in the post-embryonic stages of *Hofstenia* (Hulett et al., 2020).

Hatched-juvenile stage (193-204 hpl)

The embryo continues to occupy increasingly more space within the eggshell until it eventually breaks free as a hatched juvenile animal (Fig. 3A). Hatching occurs when the worm tears out of the eggshell. There is variability in the timing of hatching, even among embryos from the same clutch, which are presumably fertilized at approximately the same time (Movie 1). Free-swimming hatched juvenile worms move on the substrate and swim through the water column. Although most of the worms acquire brown-and-white pigmentation, there is considerable phenotypic diversity in coloration (Fig. S1E). Some individuals have little to no brown pigmentation and appear mostly translucent with white bands. Others have very little white pigmentation and are mostly brown. The white bands are not contiguous in some individuals and are entirely absent in others.

Two distinct cell-internalization events occur during *Hofstenia* development

Previous studies of acoel embryos reported a single cell-internalization event in which the vegetal macromeres are enveloped by the micromere progeny. This event is believed to represent gastrulation, because the internalized macromeres gave rise to the endomesoderm (Henry et al., 2000) and the expression of the gene *brachyury* was detected at the site of internalization (Hejnol and Martindale, 2008a). Our staging series showed that *Hofstenia* embryos likely undergo two cell-internalization events during early embryogenesis: (1) internalization of the vegetal macromeres during the gastrula stage; and (2) internalization of cells during the dimple stage (Fig. 3A; Movie 1). To facilitate better characterization of the two cellular internalization events, we used fluorescent dextran injections to visualize cells in developing embryos.

We injected the 1a and 1b micromeres of the four-cell embryo with fluorescein dextran and imaged live the stages in which cell movements were observed (Fig. 4). When viewed from the vegetal side during early cleavage (10 hpl), the two unlabeled macromeres were seen as large, dark masses. As the labeled micromeres on the animal side continued to proliferate, their daughter cells were observed moving towards the vegetal side and enveloping the two unlabeled macromeres (Fig. 4A; Movie 3). Thus, much like other acoel species, duet cleavage in *Hofstenia* concluded with the internalization of macromeres at the vegetal pole.

Next, we imaged the same micromere-injected embryos at the dimple stage in which a subset of labeled cells was observed to be internalized at the site of the dimple (Fig. 4B; Movie 4). The internalizing cells appeared to converge at a single point on the surface of the embryo. Altogether, this confirmed our initial observations that *Hofstenia* undergoes a second, previously undescribed cell-internalization event among acoels. We then performed continuous live-imaging of embryos (n=5) from the early cleavage to the dimple stage to determine where the second internalization (the dimple) occurred in relation to the animal-vegetal axis of the embryo (Movie 5). We found that the dimple forms in the animal hemisphere, approximately opposite to the site of macromere internalization (the first cell internalization) (Fig. 4C). Further studies of fate mapping in *Hofstenia* embryos are needed to determine whether either of these internalization events correspond to gastrulation (i.e. the internalization of endomesoderm) in this species.

RNA sequencing suggests major transcriptional shifts occur after the dimple stage

We next performed bulk RNA sequencing (RNA-seq) in triplicate on embryos spanning all major developmental stages to identify

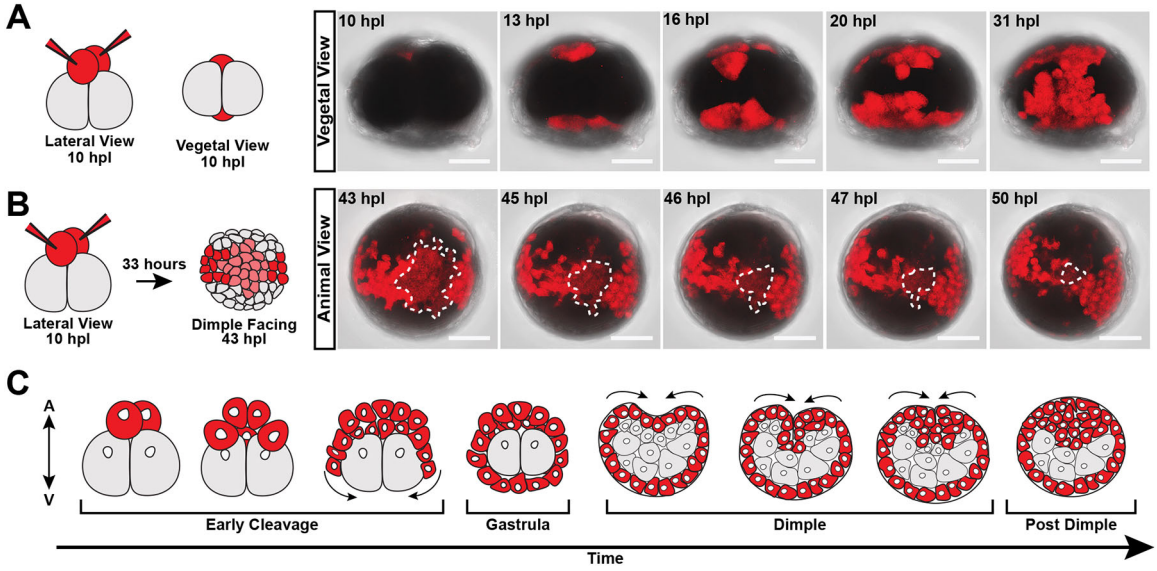

Fig. 4. Two distinct cell-internalization events occur during early development in *Hofstenia miamia*. (A) Left: schematic depicting micromeres injected with fluorescent dextran (red triangles depict microinjection needles) at the four-cell stage when viewed laterally and from the vegetal pole. Right: time-lapse screen captures of fluorescent dextran-injected embryos when viewed from the vegetal pole (Movie 3). The daughter cells of micromeres labeled in red can be seen spilling over to the vegetal side and enveloping the macromeres (n=7). (B) Left: schematic demonstrating the distribution of cells injected with fluorescent dextran (red triangles depict microinjection needles) at the dimple stage when facing the dimple. Right: time-lapse screen captures of dye-injected embryos when viewed from the animal pole during the dimple stage (Movie 4). The patch of cells outlined by a dashed white line are gradually internalized during the dimple stage (n=7). (C) Schematic depicting the two cell-internalization events during *Hofstenia* development, with all micromeres and their progeny colored in red. Scale bars: 100 µm.

Development (2021) 148, dev188656. doi:10.1242/dev.188656

molecular correlates of the stages we defined based on morphology. All early-cleavage stages were pooled and the post-dimple stage was split into two different time ranges to gain further temporal resolution of gene expression. Principal component analysis (PCA) of our samples showed that replicates within the same developmental stages were consistent, enabling us to identify key differences across stages (Fig. 5A). Based on the spatial segregation of the two earliest stages sampled (early cleavage and gastrula) on the PCA plot, we hypothesized that, globally, the transcriptomes of these stages were distinct from those of all other samples. This suggested that a major transcriptional shift occurs at, or preceding, the dimple stage, and we sought to identify the associated genes and molecular functions.

To identify key genes that may have functional significance during *Hofstenia* development, we performed pairwise differential expression analyses between consecutive developmental stages and turned our attention to genes that changed significantly in expression during at least one transition during development. We then generated a heatmap plotting normalized expression values (transcripts per million, TPM) of these genes to visualize and identify broad patterns in expression during embryogenesis (Fig. 5B). Much like the PCA plot, the heatmap highlighted that the early-cleavage and gastrula stages were similar in gene expression profile and were distinct from all other stages. The heatmap also revealed groups of genes that appeared to have similar expression dynamics across development, with hierarchical

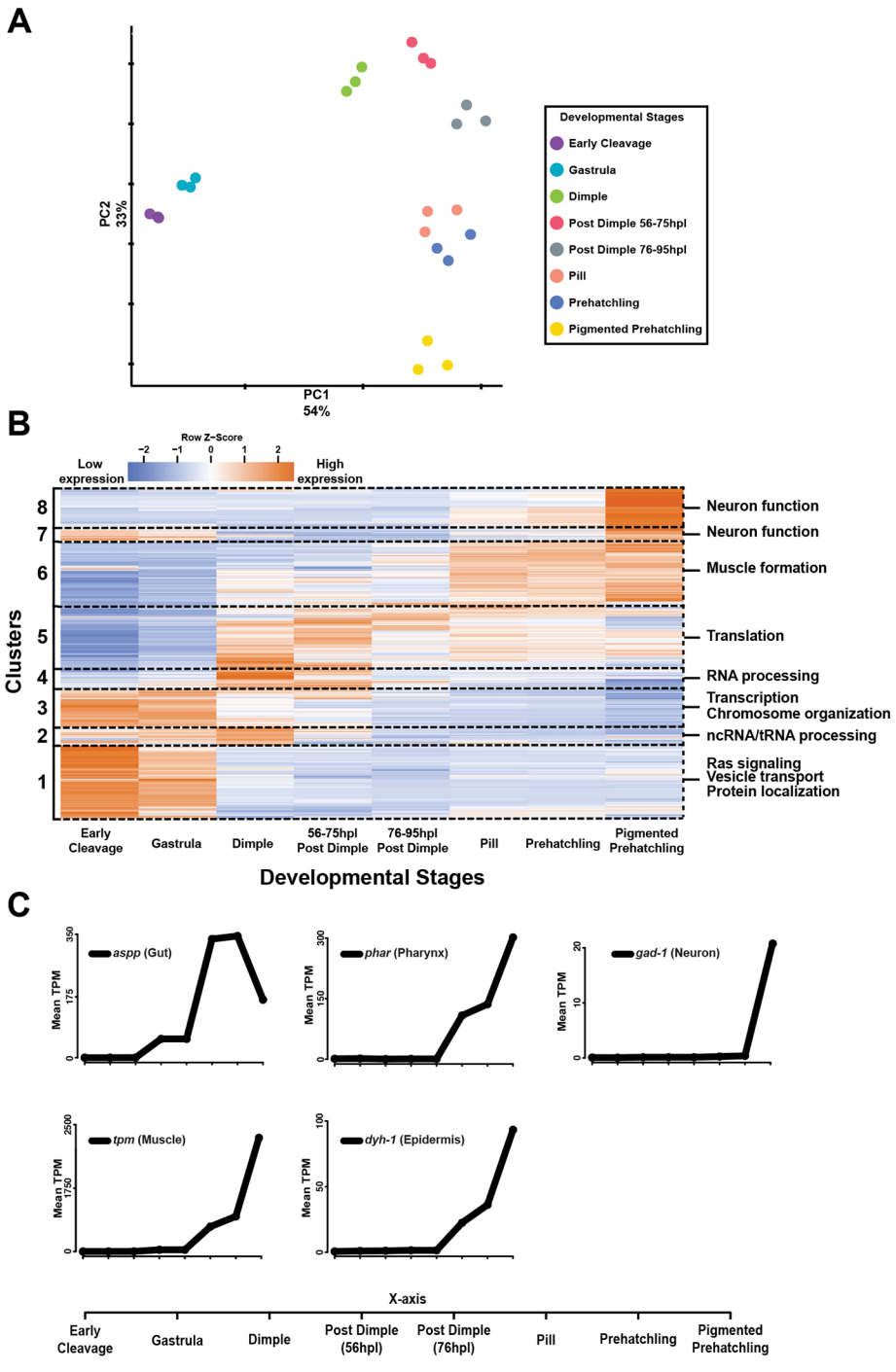

Fig. 5. Bulk RNA-seq suggests that the formation of differentiated tissues occurs only after the dimple stage in *Hofstenia miamia*. (A) PCA plot of all samples shows that the early-cleavage and gastrula stages are transcriptionally distinct from all other stages. Colors represent samples from the same developmental stage. (B) Heatmap of the mean TPM values across three biological replicates per developmental stage of genes that are significantly differentially expressed during development (likelihood ratio test). Columns represent developmental stages, whereas rows represent genes. The dashed lines demarcate gene clusters generated from hierarchical clustering that have similar expression profiles across development. Each cluster identity is labeled on the left of the heatmap. Representative GO terms associated with each cluster are listed on the right of the heatmap. (C) Mean TPM values for known differentiated tissue marker genes. All markers shown have expression levels that increase only after the dimple stage. The legend for the *x*-axis for all graphs is shown at the bottom.

Development (2021) 148, dev188656. doi:10.1242/dev.188656

clustering recovering eight clusters with distinct patterns of expression.

We next sought to determine whether genes associated with specific functional roles could be enriched in these gene clusters. Thus, we used gene ontology (GO) enrichment analysis to capture any associated molecular functions (Fig. 5B; Table S2A). We found that clusters containing genes that became highly expressed starting during the dimple stage were enriched for terms associated with translation, RNA processing and muscle formation. Terms associated with neuronal function were highly enriched in cluster 8, where the majority of the genes appeared to be highly expressed only late in development, at the pigmented-prehatchling stage. Another cluster, cluster 7, showed weak enrichment for terms associated with neuronal biology, but contained genes with high expression during early and late stages of development, suggesting that some biological processes underlying neurons may be used in early embryonic cells. The enrichment of terms associated with neuronal function and muscle formation among genes with elevated expression after the dimple stage suggested that differentiated cell types were only present after this stage.

To confirm the GO enrichment analysis results and to expand on the hypothesis that differentiated cell types are only present after the dimple stage, we examined the mean TPM values of known differentiated cell type markers across development (Fig. 5C). We found that all markers examined [gut, *lysosomal aspartic protease* (*aspp*); neuron, *glutamate decarboxylase* (*gad-1*); epidermis, *dynein heavy chain-1* (*dyh-1*); pharynx, *pharynx* (*phar*); and muscle, *tropomyosin* (*tpm*)] increased in expression levels only after the dimple stage. Furthermore, the expression profile of the muscle marker *tpm* and of the neural marker *gad-1* mirror the expression profile of cluster 6 and of cluster 8, which were found to be enriched for terms associated with muscle formation and neuronal function, respectively. This suggests that organogenesis and substantial gene expression changes in the embryo occur after the dimple stage, further highlighting the potential importance of the associated internalization event.

Cells expressing differentiated cell markers and body axes appear after the dimple stage

We performed *in situ* hybridization of the differentiated tissue markers examined above to assess the hypothesis that these markers are expressed only after the dimple stage and to determine where within the embryo these markers are expressed. We found that the expression of gut, muscle, epidermis, pharynx and neural markers were all detected after the dimple stage (Fig. 6A-C).

During the hatched-juvenile stage, *aspp* marked the gut, revealing cells that were closely associated with one another in the internal region of the worm (Fig. 6B). In embryos, *aspp* expression was detected among a tight cluster of cells that occupied the center of the embryo starting during the early post-dimple stage (60 hpl). Imaging at higher magnification showed an increase in the abundance of these cells with time.

The muscle marker *tpm* marked a mesh-like network of orthogonal muscle fibers that were present in the subepidermal periphery and pharynx of the hatched juvenile-stage worm (Fig. 6B; Fig. S6). Among embryos, *tpm* also occupied the subsurface periphery and was first detected during the late post-dimple stage (80 hpl) (Fig. 6B; Fig. S6). High-magnification imaging revealed the gradual emergence of cellular extensions starting during the pill stage, which ultimately formed a mesh-like network during the late pigmented-prehatchling stage (150-160 hpl) resembling that of the hatched-juvenile stage. This suggests that, although cells that express *tpm* are present as early as the post-dimple stage (80 hpl), they do not necessarily adopt the morphology of mature muscle tissue until very late in development.

The *Hofstenia*-specific gene *phar* clearly labeled both the opening and internal structure of the pharynx during the hatched-juvenile stage (Fig. 6B). This gene was detected during the pill stage as a patch of cells on the presumptive anterior of the embryo. As the embryo developed further, *phar* was observed in a tube-like pattern that extended internally from the outer surface of the embryo (Fig. 6B,C). The timing of *phar* expression in a pharynx-like pattern matched with when we were able to detect the formation of the mouth in our live-imaging and developmental atlas (Fig. 3A; Movie 1).

The epidermal marker *dyh-1* was expressed in the epidermis of the hatched juvenile worm (Fig. 6B). Expression was detected on the outer periphery of the embryo from the prehatchling stage onward. High-magnification images confirmed that *dyh-1* was only expressed in the outermost cell layer and that this expression was maintained until hatching. This suggested that *dyh-1* marks the cells that ultimately become the mature epidermis. Finally, the neural marker *gad-1* marks the anterior condensation and body neurons in hatched worms, as described by Hulett et al. (2020). During development, this gene was only detectable during the late pigmented-prehatchling stage (150-160 hpl), with the distribution of signal resembling that of a hatched-juvenile stage. Higher-magnification images confirmed the presence of axon-like extensions in both the pigmented-prehatchling stage and hatched-juvenile stage.

The timing or stage of detection of these markers through *in situ* hybridization corroborated the temporal dynamics of the expression levels of these genes as revealed by the RNA-seq data discussed above (Fig. 5C, Fig. 7). Additionally, the markers that were detected correspond to tissues derived from all three germ layers that are present among bilaterian animals. This could suggest that the specification of the three germ layers occurs after the dimple stage. However, we cannot rule out the possibility that germ layers are specified earlier, possibly even before the dimple stage, with differentiated cell-type markers becoming expressed only later in development. Once the markers of differentiated cell types were observable, we noted substantial changes in these tissues. For example, gut, muscle and pharyngeal cells became more numerous and organized into distinct structures (Fig. 6B). Based on these data, we infer that organogenesis occurs after the dimple stage.

With the organization of tissues becoming more apparent during the post-dimple stage, we next determined when and where genes involved in specifying body axes were expressed. Among bilaterally symmetric animals, genes implicated in axis formation are expressed on opposite poles during early development, often before or during gastrulation (Petersen and Reddien, 2009; Sasai et al., 1994). It has been established that, in adult *Hofstenia*, Wnt and Wnt antagonists are expressed in a polarized manner along the AP axis and *bmp* and the Bmp antagonist *admp* are expressed on the dorsal and ventral (DV) sides, respectively (Srivastava et al., 2014). During *Hofstenia* embryogenesis, double *in situ* hybridization revealed that the anterior marker *sfrp-1* and posterior marker *fz-1* occupy distinct, opposite territories during the pill stage, suggesting that the AP axis has been established by this stage (Fig. S5A,B). *admp* and *bmp* were also detectable at opposite sides from the pill stage onwards, indicating the presence of a clear DV axis (Fig. S5A,B). Furthermore, our gene expression studies showed that the AP and DV axes are present in the correct spatial relationship to each other by the pill stage (Fig. S5A,B).

Development (2021) 148, dev188656. doi:10.1242/dev.188656

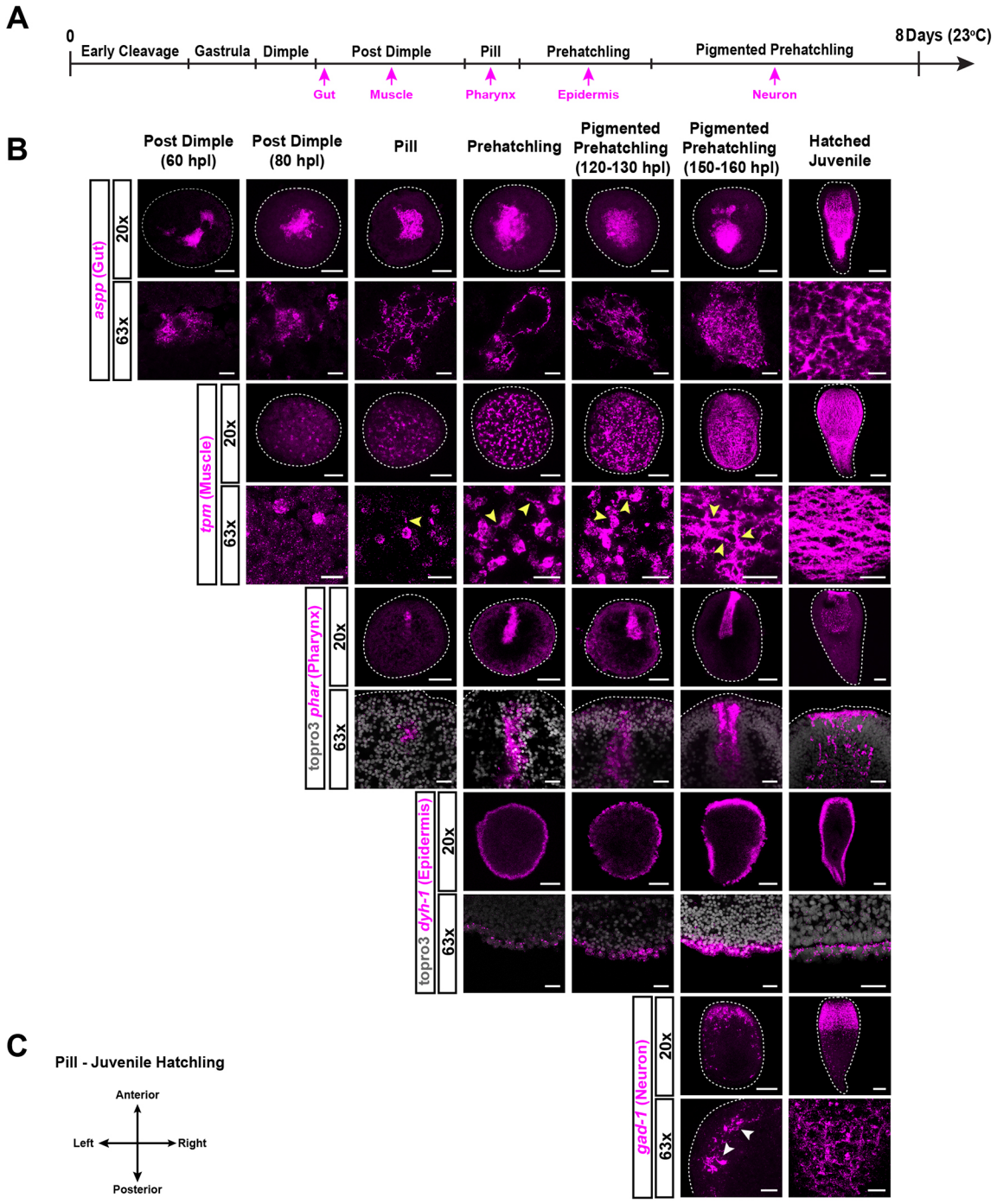

Fig. 6. Expression of differentiated tissue marker genes is detected after the dimple stage. (A) Schematic timeline of development showing when markers for differentiated cell types were first detected via *in situ* hybridization. (B) *In situ* hybridization of differentiated cell markers. *aspp* marked the gut in the hatched juvenile worms (*z*-projection) and internal cells in embryos (optical section) starting from the post-dimple stage (60 hpl). *tpm* marked muscle in the hatched juvenile worms (*z*-projection), showing a mesh-like network of muscle fibers. Expression was first detected at the post-dimple stage (80 hpl) and cells started to exhibit fiber-like projections during the pill stage (yellow arrowheads) (optical section). The pharynx marker *phar* was first detected during the pill stage as a patch of cells on one side of the embryo (optical section). This patch of expression changed into a tube-like structure that extended internally during the prehatchling stage, outlining the pharynx. The nuclear stain TO-PRO-3 was used in the 63× magnification images to visualize the outer boundaries of the embryo. *dyh-1* marked the epidermis in the hatched juvenile (optical section) and expression was detected in the outermost cells of the embryos during the prehatchling stage (optical section). *gad-1* marked neural cell types in the hatched juvenile (z-projection), showing a high condensation of cells in the anterior compared with a more-diffuse pattern of expression throughout the rest of the body. *gad-1* was only detected in the 150-hpl pigmented-prehatchling stage (*z*-projection), showing expression patterns resembling those of the hatched juveniles, with axon-like extensions being visible (white arrows). Dashed lines represent the outer boundary of embryos and hatched juveniles. (C) Orientation of embryos from pill to hatched-juvenile stages. Axes orientation for the post-dimple stage was not possible because of the lack of morphological landmarks. Scale bars: 100 µm (20× magnification) and 25 µm (63× magnification) in B.

Development (2021) 148, dev188656. doi:10.1242/dev.188656

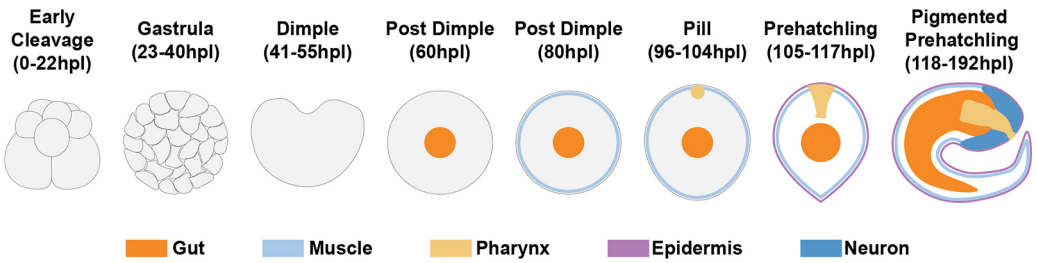

Fig. 7. Schematic summarizing the major developmental stages and formation of differentiated tissues in *Hofstenia miamia*. During *Hofstenia* development, the gut is first detected in the center of the embryo (orange). Next, muscle is detected in the subsurface periphery of the embryo (light blue). The pharyngeal marker is then detected in a small patch on the surface of the embryo (yellow). The epidermal marker is detected during the pill stage (purple). Finally, neurons are detected during the pigmented-prehatchling stage internally on the anterior side of the embryo (dark blue).

DISCUSSION

This study provides an in-depth characterization of embryogenesis of the acoel worm *H. miamia*. *Hofstenia* embryos undergo duet cleavage, a stereotyped form of early embryonic development that is specific to acoels. Although all duet cleavage programs involve the formation of a 'duet' of animal pole micromeres and a pair of vegetal pole macromeres, acoel species display variations in the number, order and symmetries of cleavages. We found that *Hofstenia* embryos cleave in a stereotyped pattern similar to those of the convolutid species *Neochildia fusca*, *Convolutriloba longifissura* and *Symsagittifera roscoffensis*, but with some differences (Bresslau, 1909; Hejnol and Martindale, 2008a; Henry et al., 2000). At the four-cell stage in *Hofstenia*, the micromeres 1a and 1b cleave before the 1A and 1B macromeres, whereas the macromeres cleave before the micromeres in convolutids. Moreover, the cleavage of the 1a and 1b micromeres in *Hofstenia* is asymmetric, differing from the symmetric cleavage of the corresponding micromeres observed in convolutids. Furthermore, macromeres 3A and 3B are internalized at the 16-cell stage in convolutids. In *Hofstenia*, the macromeres are not fully internalized until after subsequent cell divisions. Internalization of the vegetal macromeres in *Hofstenia* embryos started only after the 16-cell stage was reached (Movie 2). *Hofstenia* and convolutid cleavage programs show similarities to development in nemertodermatids, which also form a four-cell stage with paired vegetal macromeres and animal micromeres; however, subsequent cleavage in nemertodermatids is different (Børve and Hejnol, 2014). Given that *Hofstenia* represents a sister group to the vast majority of acoels, whereas convolutids diverged later within the clade (Jondelius et al., 2011), we infer that the conserved features of duet cleavage in acoels include the formation of a pair of vegetal macromeres that cleave counter-clockwise and asymmetrically to form 'duets' of smaller micromeres on the animal side, which ultimately envelop the vegetal macromeres. Fate-mapping studies in multiple species are needed to assess whether the shared macromere-micromere organization of the embryos represents conserved specification events across acoels.

The duet cleavage pattern observed in *Hofstenia* and other acoel embryos is reminiscent of spiral cleavage, which involves the formation of four vegetal macromeres that produce 'quartets' of micromeres toward the animal pole. The former placement of acoels within the spiralian phylum Platyhelminthes and the striking similarities between spiral and duet cleavage suggested that duet cleavage is a derived form of spiral (Ax and Dörjes, 1966; Ax and Jeffries, 1987; Boyer et al., 1996; Boyer and Jonathan, 1998; Bresslau, 1909; Costello and Henley, 1976; Henry and Martindale, 1999; Hyman, 1951; Peterson and Eernisse, 2001; Smith et al., 1986). With molecular phylogenies now consistently placing acoels as distantly related to Platyhelminthes, duet cleavage should not be studied with an assumption of homology to spiral cleavage (Hejnol et al., 2009; Jondelius et al., 2011; Kapli and Telford, 2020; Marlétaz et al., 2019; Mwinyi et al., 2010; Philippe et al., 2007, 2011, 2019; Ruiz-Trillo et al., 1999, 2002, 2004; Ruiz-Trillo and Paps, 2016; Sempere et al., 2007; Telford et al., 2003). Given the similarities between these distantly related lineages, detailed comparisons of the cell and molecular processes of spiral and duet cleavage would uncover whether shared or divergent mechanisms underlie seemingly related cleavage programs. *Hofstenia* embryos, which are amenable to experimental manipulations, will facilitate systematic comparisons of duet and spiral cleavage programs.

Our developmental atlas showed that, after duet cleavage is completed, *Hofstenia* undergoes two cell-internalization events. The first of these cell-internalization events occurs through the movement of animal pole micromeres, which results in internalization of the vegetal macromeres. Previous work defined gastrulation in acoels as the internalization of the macromeres, a direct parallel to the mechanism of gastrulation in some spiralian embryos (Apelt, 1969; Bresslau, 1909; Hejnol and Martindale, 2008a; Henry et al., 2000). However, spiralians undergo gastrulation in different modes, despite their conserved cleavage program (e.g. epiboly and invagination at different stages of development) (Lambert, 2010; Lyons and Henry, 2014). It is possible that, even among acoels, the mode of gastrulation differs widely. Therefore, it will be important to confirm that the internalized macromeres in *Hofstenia* give rise to endomesoderm. The second internalization event in *Hofstenia*, which had not been described previously in other acoel species, occurs at the dimple stage at the animal pole. It is unknown whether this second internalization has remained undetected in previously studied species, or whether *Hofstenia* represents a unique instance in which a second internalization event occurs at the dimple stage. Our work shows that this cellular event corresponds to a major transcriptional shift in which the gene expression profile becomes distinct from that of the earlier early-cleavage and gastrula stages. Moreover, GO enrichment analysis and *in situ* hybridization data detected the expression of differentiated tissue-marker genes corresponding to all three germ layers only after the dimple stage (Fig. 5C, Figs 6, 7). Fate mapping of cells internalized at the dimple stage will reveal whether this internalization could also represent a gastrulation-like event in *Hofstenia*.

Our *in situ* hybridization data showed when major body axes and differentiated tissue types become detectable during *Hofstenia* embryogenesis. Previous studies of other acoel species have highlighted the formation of muscle fibers and the expression of neural transcription factors during embryonic development (Ladurner and Riger, 2000; Semmler et al., 2008; Perea-Atienza et al., 2018). We found that the pattern by which *Hofstenia* muscle cell extensions form differs from the process of muscle formation in

Development (2021) 148, dev188656. doi:10.1242/dev.188656

other acoels, such as *S. roscoffensis* and *Convoluta pulchra*. In *C. pulchra*, circular, latitudinal muscle fibers appear first and are later connected by longitudinal fibers (Ladurner and Rieger, 2000). Myogenesis in *S. roscoffensis* occurs by the formation of muscle fibers sequentially from the animal to the posterior pole (Semmler et al., 2008). We did not observe sequential formation of muscle in *Hofstenia*. Instead, the fibers were first distributed in random directions and across all parts of the embryo and then resolved into an organized lattice by 150 hpl. Formation of neurons has been inferred via studies of the expression of basic helix-loop-helix (BHLH) transcription factors, often associated with neurogenesis, in the embryos of *S. roscoffensis* (Perea-Atienza et al., 2018). In *S. roscoffensis*, the majority of the BHLH transcription factors tested were expressed within the first 24 h of development. This represents expression at an early stage, given that it takes 4-5 days for this species to complete embryogenesis. This study most likely found early progenitors of neurons, whereas our study focused on identifying when mature neurons were present. Studies of neural transcription factor expression in *Hofstenia* embryos are needed to determine when neural progenitors are present in this species.

It will also be important to determine the source of progenitors of differentiated tissues during development, given the biology of adult *Hofstenia*. By the time they hatch, the worms have a population of pluripotent stem cells known as neoblasts, which are the source of new cells for homeostatic tissue turnover and regeneration (Srivastava et al., 2014). Given the stereotyped cleavage pattern and cell-internalization events observed in *Hofstenia*, it could be possible that *Hofstenia* undergoes a transition from the 'classic' mode of development, in which the adult body plan is derived through the formation of germ layers, to a 'neoblast' mode of development, in which tissues become derived through the differentiation of a neoblast population. Future work on the fate map of early blastomeres as well as cell-cycle behavior during embryogenesis will illuminate this question.

Our study represents the first step in establishing *Hofstenia* embryos as a new acoel model for developmental biology. *Hofstenia* represents a genomically enabled, early-diverging member of the acoel clade, making its embryos an attractive system for functional studies that inform the evolution of development (Gehrke et al., 2019; Jondelius et al., 2011; Srivastava et al., 2014). Furthermore, given the capacity of *Hofstenia* for whole-body regeneration, its embryos can also be used to address questions of stem cell specification, maintenance and differentiation.

MATERIALS AND METHODS

Hofstenia miamia adult and embryo culturing

The laboratory population of *H. miamia* adults represent many generations derived from 120 sexually reproducing worms collected from Bermuda in 2010 (Srivastava et al., 2014). The embryos used in this study were the progeny of random matings of these worms, making them a polymorphic, lab-bred population. *Hofstenia* adults were cultured in plastic boxes (20-30 adults in 1 l of artificial seawater) at 21°C and embryos were found to be laid on the plastic in clutches (Fig. S1B,C). Embryos were laid spontaneously, with typical clutch sizes being four to seven embryos. These clutches can be as few as one, or as many as 30 embryos. Artificial seawater for culturing both adults and embryos was made by diluting Instant Ocean Sea Salt Mix (Instant Ocean Product no. SS15-10) with deionized water to obtain a solution with a salinity of 37 ppt and pH 7.8-8.0. Upon reaching sexual maturity, *Hofstenia* adults retain a high embryo production rate for 6-8 months. However, given proper care, we have found that adults over 1 year old will still produce enough embryos to support experiments. Worms were fed and cleaned twice a week. Typically, adults produce approximately four embryos per week (Srivastava et al., 2014).

Embryos were collected using a glass Pasteur pipette. Embryos at the two- and four-cell stages were sorted manually under a dissection microscope and incubated at 23°C until the desired stage was reached. Embryos were cultured at this higher temperature, which corresponds to room temperature in our laboratory, to maintain consistency in the timing of developmental milestones detected in time-lapse imaging, which was conducted at room temperature (Movie 1). Embryos were staged based on morphological changes observed under a dissecting microscope (Leica, MDG41) and developmental timing was determined based on the number of hpl estimated at 23°C.

Embryo deshelling and fixation

In order to allow *in situ* probes and small molecules to penetrate the egg shell, embryos were treated while on a shaker with a deshelling solution (32 mM sodium hydroxide, 0.5 mg/ml sodium thioglycolate and 1 mg/ml of pronase in artificial seawater) for varying times depending on the developmental stage. Embryos from early cleavage to pill stages were incubated for 8 min, whereas prehatchling and pigmented-prehatchling stages were incubated for 6 min. Once treated, embryos were fixed in 4% paraformaldehyde solution in seawater overnight at 4°C. After fixation, embryos were stored in PBS at 4°C for a maximum of 1 week before use in *in situ* hybridization.

Dye injections

A plastic mold with 300 µm pins was made using a laser cutter. This mold was placed in molten 1% agarose. Once the agarose solidified, the pins created small holes into which embryos were placed. Embryos were then injected with fluorescein dextran using a Narishige micromanipulator connected to a Harvard Apparatus injector and quartz needles (Sutter Instrument GF100-50-10).

Live imaging

Time-lapse imaging was carried out at 23°C, because the room in which we performed the imaging was kept at a constant 23°C. Embryos were mounted on glass slides underneath coverslips with 'clay feet'. The slides were then sealed using Vaseline. Embryos that were injected with fluorescein dextran were imaged with a Leica SP8 confocal microscope at intervals of 10 min. For Movies 1, 2 and 5, images were taken at intervals of 2, 5 and 10 min, respectively under a Leica DM8000 stereomicroscope.

RNA sequencing

RNA was extracted from eight stages (early cleavage, gastrula, dimple, post-dimple 56-75 hpl, post-dimple 76-95 hpl, pill, prehatchling and pigmented prehatchling) using the Nucleospin RNA XS kit (MACHEREY-NAGEL). To obtain enough total RNA to synthesize libraries, multiple embryos (~90-100) were pooled to generate a single biological replicate for each stage. Three biological replicates were made for each developmental stage. RNA-seq libraries were generated using the Illumina TruSeq RNA Library Prep kit v2. Libraries were analyzed for quality using the Agilent Tapestation High Sensitivity D1000 tape and were subsequently used for single-end, 75 bp sequencing in one lane of the Illumina NextSeq sequencer.

Libraries were demultiplexed and reads were pseudo-mapped and quantified using Salmon (Patro et al., 2017). Salmon outputs were then converted into a format that can be used by Sleuth using the R package Wasabi (https://github.com/COMBINE-lab/wasabi). Differential expression was determined with the R package Sleuth (https://github.com/pachterlab/sleuth) using the likelihood ratio test (Pimentel et al., 2017). Differential expression analysis was performed in a sequential fashion, performing pairwise comparisons of developmental stages adjacent in time to one another. Differential expression was called by setting a q value cutoff of 0.05, with the exception of the comparison between pill and prehatchling stages, where a *P*-value cutoff of 0.05 was used (Table S2B). This different criterion was used for these stages because differential expression analysis yielded no genes that retained statistical significance after multiple test correction (false discovery rate adjusted *P*-value). This lack of significance between the pill and prehatchling stages may be because the two stages have a similar transcriptomic profile. Regardless, the noncorrected *P*-values provided an ordered list of genes, which was used for our analyses. All hierarchical

clustering and heatmap generation was performed using the gplots package in R (R Project). The heatmap was generated using a matrix of TPM values of genes with at least one statistically significant difference when comparing consecutive stages during development (Table S2C). Hierarchical clustering was done using the WardD clustering method on this matrix using the hclust function. PCA was performed on the Sleuth object generated using estimated counts. Generation of line graphs depicting mean TPM values across three biological replicates was performed in R using a custom script. All mean TPM values were calculated by taking the mean of the TPM values in each biological replicate for each developmental stage (Table S2D). GO enrichment analysis was performed using the DAVID functional annotation tool (Table S2A). The best BLAST hits by e-value for *Hofstenia* genes against humans were used to perform GO enrichment analysis. The *Hofstenia* transcriptome was used as the background in this analysis. R scripts that were used to determine differential expression, generate plots and perform hierarchical clustering are available at https://github.com/JulianKimura/R_scripts. These transcriptome data are available through an interactive web-interface via http://n2t.net/ark:/84478/d/fzht4sx3. Note that the DrEdGE analysis used different statistical approaches, but produced comparable results.

Gene cloning

All genes were annotated based on the best BLAST hit by e-value against human genes and were given UniProt identifiers. Genes of interest were amplified and cloned using the methods described by Srivastava et al. (2014). Genes were named using BLAST-based sequence similarity to known proteins; their corresponding primer and sequence information is listed in Table S1.

In situ hybridization

All tissue markers used in this study were chosen based on previous screens performed in our lab. Riboprobes used for *in situ* hybridization were synthesized using the methods described by Pearson et al. (2009). An adjusted version of the *in situ* hybridization protocol mentioned by Srivastava et al. (2014) was used on deshelled and fixed embryos. During the proteinase K step, embryos were treated for varying times depending on the stage, 1 min for 0-107 hpl-hatched juveniles and 3 min for 108 hpl-hatched juveniles. The pre-hybridization and hybridization solutions were made using 8 M urea instead of DI formamide (Sinigaglia et al., 2018). With the exception of Fig. S3A, which was stained with DAPI, all nuclei were stained using a TO-PRO-3 Iodide (642/661) (Thermo Fisher Scientific).

Phalloidin and cell mask staining

Phalloidin staining was performed on deshelled and fixed embryos using the methods described by Srivastava et al. (2014). CellMask Green Plasma Membrane Stain (Invitrogen) was used to visualize cilia on the surface of embryos at the pill stage. CellMask was used at a 1:1000 dilution in artificial seawater from a 1000× stock solution in DMSO. Embryos were first deshelled for the appropriate amount of time depending on the stage, as described above, and placed in the CellMask solution for 2 h at room temperature. The embryos were then washed twice in fresh artificial seawater and imaged live.

Acknowledgements

The optimization of microinjections was carried out with the help of Dr Mark Martindale. We thank Dr Seth Donoughe and Dr Cassandra Extavour for helpful discussions, for making the embryo microinjection molds and for inspiration for the developmental time series. Thank you to Patrick Golden for generating an online resource to host our bulk RNA-seq dataset. We also thank Dr Andrew Gehrke, Dr Marcela Bolaños, Dr Yi Jyun Luo, Dr Alyson Ramirez, Ryan Hulett and Dr Deirdre Lyons for helpful discussions. Finally, we would like to acknowledge the intellectual and technical support from all members of the Srivastava Lab.

Competing interests

The authors declare no competing or financial interests.

Author contributions

Conceptualization: J.O.K., L.R., M.S.; Methodology: J.O.K., M.S.; Validation: J.O.K., L.R.; Formal analysis: J.O.K.; Investigation: J.O.K., L.R.; Resources: M.S.; Data curation: J.O.K.; Writing - original draft: J.O.K.; Writing - review & editing: J.O.K., L.R., M.S.; Visualization: J.O.K., L.R.; Supervision: M.S.; Project administration: J.O.K., M.S.; Funding acquisition: M.S.

Funding

This work was supported by grants to M.S. from the Searle Scholars Program, the Richard and Susan Smith Family Foundation and the National Institutes of Health (1R35GM128817). J.K. is supported by the National Science Foundation-Simons Center for Mathematical and Statistical Analysis of Biology at Harvard and the Harvard Quantitative Biology Initiative (1764269). Deposited in PMC for release after 12 months.

Data availability

RNA-seq data are available at http://n2t.net/ark:/84478/d/fzht4sx3. Raw fastq files of the embryonic transcriptome have been deposited in the NCBI Sequence Read Archive under the bioproject code PRJNA603318. Gene sequences have been submitted to Genbank under accession numbers MZ398249, MZ398250 and MZ398251.

Peer review history

The peer review history is available online at https://journals.biologists.com/dev/article-lookup/doi/10.1242/dev.188656

References

Apelt, G. (1969). Fortpflanzungsbiologie, Entwicklungszyklen und vergleichende Frühentwicklung acoeler Turbellarien. *Mar. Biol.* **4**, 267-325.

Arendt, D., Technau, U. and Wittbrodt, J. (2001). Evolution of the bilaterian larval foregut. *Nature* **409**, 81-85. doi:10.1038/35051075

Ax, P. and Dörjes, J. (1966). Oligochoerus limnophilus nov. spec., ein kaspisches Faunenelement als erster Süßwasservertreter der Turbellaria Acoela in Flüssen Mitteleuropas. *Int. Rev. Ges. Hydrobiol. Hydrogr.* **51**, 15-44. doi:10.1002/iroh.19660510104

Ax, P. and Jeffries, R. P. S. (1987). The phylogenetic system: the systematization of organisms on the basis of their phylogenesis. Wiley New York. Available at: https://pdfs.semanticscholar.org/be84/045da27d1f14174891a91c9b53e643470dc6.pdf.

Baguna, J., Salo, E. and Auladell, C. (1989). Regeneration and pattern formation in planarians. III. that neoblasts are totipotent stem cells and the cells. *Development* **107**, 77-86. doi:10.1242/dev.107.1.77

Børve, A. and Hejnol, A. (2014). Development and juvenile anatomy of the nemertodermatid Meara stichopi (Bock) Westblad 1949 (Acoelomorpha). *Front. Zool.* **11**, 50. doi:10.1186/1742-9994-11-50

Bourlat, S. J. and Hejnol, A. (2009). Acoels. *Curr. Biol.* **19**, R279-R280. doi:10.1016/j.cub.2009.02.045

Boyer, B. C. (1971). Regulative development in a spiralian embryo as shown by cell deletion experiments on the Acoel, Childia. *J. Exp. Zool.* **176**, 97-105. doi:10.1002/jez.1401760110

Boyer, B. C. and Jonathan, Q. H. (1998). Evolutionary modifications of the spiralian developmental program. *Am. Zool.* **38**, 621-633. doi:10.1093/icb/38.4.621

Boyer, B. C., Henry, J. Q. and Martindale, M. Q. (1996). Modified spiral cleavage: the duet cleavage pattern and early blastomer fates in the acoel turbellarian neochildia fusca. *Biol. Bull.* **191**, 285-286. doi:10.1086/BBLv191n2p285

Bresslau, E. (1909). Die Entwicklung der Acoelen. *Deutsche Zoologische Gesellschaft* **19**, 314-324.

Costello, D. P. and Henley, C. (1976). Spiralian development: a perspective. *Am. Zool.* **16**, 277-291. doi:10.1093/icb/16.3.277

Davies, E. L., Lei, K., Seidel, C., Kroesen, A. E., Mckinney, S. A., Guo, L., Robb, S. M. C., Ross, E. J., Gotting, K. and Alvarado, A. S. (2017). Embryonic origin of adult stem cells required for tissue homeostasis and regeneration. *eLife* **6**, e21052. doi:10.7554/eLife.21052

Eisenhoffer, G. T., Kang, H. and Sánchez Alvarado, A. (2008). Molecular analysis of stem cells and their descendants during cell turnover and regeneration in the planarian Schmidtea mediterranea. *Cell Stem Cell* **3**, 327-339. doi:10.1016/j.stem.2008.07.002

Gehrke, A. R. and Srivastava, M. (2016). Neoblasts and the evolution of whole-body regeneration. *Curr. Opin. Genet. Dev.* **40**, 131-137. doi:10.1016/j.gde.2016.07.009

Gehrke, A. R., Neverett, E., Luo, Y.-, Brandt, A., Ricci, L., Hulett, R. E., Gompers, A., Ruby, J. G., Rokhsar, D. S., Reddien, P. W., et al. (2019). Acoel genome reveals the regulatory landscape of whole-body regeneration. *Science* **363**, eaau6173. doi:10.1126/science.aau6173

Hejnol, A. and Martindale, M. Q. (2008a). Acoel development indicates the independent evolution of the bilaterian mouth and anus. *Nature* **456**, 382-386. doi:10.1038/nature07309

Hejnol, A. and Martindale, M. Q. (2008b). Acoel development supports a simple planula-like urbilaterian. *Philos. Trans. R. Soc. Lond. B Biol. Sci.* **363**, 1493-1501. doi:10.1098/rstb.2007.2239

Hejnol, A. and Pang, K. (2016). Xenacoelomorpha's significance for understanding bilaterian evolution. *Curr. Opin. Genet. Dev.* **39**, 48-54. doi:10.1016/j.gde.2016.05.019
Hejnol, A., Obst, M., Stamatakis, A., Ott, M., Rouse, G. W., Edgecombe, G. D., Martinez, P., Baguñà, J., Bailly, X., Jondelius, U. et al. (2009). Assessing the root of bilaterian animals with scalable phylogenomic methods. *Proc. R. Soc. B* **276**, 4261-4270. doi:10.1098/rspb.2009.0896
Henry, J. J. and Martindale, M. Q. (1999). Conservation and innovation in spiralian development. *Hydrobiologia* **402**, 255-265. doi:10.1023/A:1003756912738
Henry, J. Q., Martindale, M. Q. and Boyer, B. C. (2000). The unique developmental program of the acoel flatworm, Neochildia fusca. *Dev. Biol.* **220**, 285-295. doi:10.1006/dbio.2000.9628
Hulett, R. E., Potter, D. and Srivastava, M. (2020). Neural architecture and regeneration in the acoel Hofstenia miamia. *Proc. Biol Sci. R. Soc.* **287**, 20201198. doi:10.1098/rspb.2020.1198
Hyman, L. (1951). *The Invertebrates: Platyhelminthes and Rhynchocoela*, Vol. II. New York: McGraw-Hill Book Company, Inc.
Jondelius, U., Wallberg, A., Hooge, M. and Raikova, O. I. (2011). How the worm got its pharynx: phylogeny, classification and Bayesian assessment of character evolution in Acoela. *Syst. Biol.* **60**, 845-871. doi:10.1093/sysbio/syr073
Kapli, P. and Telford, M. J. (2020). Topology-dependent asymmetry in systematic errors affects phylogenetic placement of Ctenophora and Xenacoelomorpha. *Sci. Adv.* **6**, eabc5162. doi:10.1126/sciadv.abc5162
Kapli, P., Natsidis, P., Leite, D., Fursman, M., Jeffrie, N., Rahman, I. A., Philippe, H., Copley, R. R. and Telford, M. J. (2021). Lack of support for Deuterostomia prompts reinterpretation of the first Bilateria. *Sci. Adv.* **7**, eabe2741. doi:10.1126/sciadv.abe2741
Ladurner, P. and Rieger, R. (2000). Embryonic muscle development of Convoluta pulchra (Turbellaria–Acoelomorpha, Platyhelminthes). *Dev. Biol.* **222**, 359-375. doi:10.1006/dbio.2000.9715
Lambert, J. D. (2010). Developmental patterns in spiralian embryos. *Curr. Biol.* **20**, R72-R77. doi:10.1016/j.cub.2009.11.041
Lyons, D. C. and Henry, J. Q. (2014). Ins and outs of Spiralian gastrulation. *Int. J. Dev. Biol.* **58**, 413-428. doi:10.1387/ijdb.140151dl
Marlétaz, F., Peijnenburg, K. T. C. A., Goto, T., Satoh, N. and Rokhsar, D. S. (2019). A new spiralian phylogeny places the enigmatic arrow worms among gnathiferans. *Curr. Biol.* **29**, 312-318.e3. doi:10.1016/j.cub.2018.11.042
Maslakova, S. A., Martindale, M. Q. and Norenburg, J. L. (2004). Vestigial prototroch in a basal nemertean, Carinoma tremaphoros (Nemertea; Palaeonemertea). *Evol. Dev.* **6**, 219-226. doi:10.1111/j.1525-142X.2004.04027.x
Mwinyi, A., Bailly, X., Bourlat, S., Jondelius, U., Littlewood, D. T. J. and Podsiadlowski, L. (2010). The phylogenetic position of Acoela as revealed by the complete mitochondrial genome of Symsagittifera roscoffensis. *BMC Evol. Biol.* **10**, 309. doi:10.1186/1471-2148-10-309
Nielsen, C. (1995). *Animal Evolution: Interrelationships of the Living Phyla*. Oxford University Press.
Patro, R., Duggal, G., Love, M. I., Irizarry, R. A. and Kingsford, C. (2017). Salmon provides fast and bias-aware quantification of transcript expression. *Nat. Methods* **14**, 417-419. doi:10.1038/nmeth.4197
Pearson, B. J., Eisenhoffer, G. T. and Gurley, K. A. (2009). Formaldehyde–based whole–mount in situ hybridization method for planarians. *Dev. Dyn.* **238**, 443-450. doi:10.1002/dvdy.21849
Perea-Atienza, E., Sprecher, S. G. and Martínez, P. (2018). Characterization of the bHLH family of transcriptional regulators in the acoel S. roscoffensis and their putative role in neurogenesis. *EvoDevo* **9**, 8. doi:10.1186/s13227-018-0097-y
Petersen, C. P. and Reddien, P. W. (2009). Wnt signaling and the polarity of the primary body axis. *Cell* **139**, 1056-1068. doi:10.1016/j.cell.2009.11.035
Peterson, K. J. and Eernisse, D. J. (2001). Animal phylogeny and the ancestry of bilaterians: inferences from morphology and 18S rDNA gene sequences. *Evol. Dev.* **3**, 170-205. doi:10.1046/j.1525-142x.2001.003003170.x
Philippe, H., Brinkmann, H., Martinez, P., Riutort, M. and Baguñà, J. (2007). Acoel flatworms are not platyhelminthes: evidence from phylogenomics. *PloS one* **2**, e717. doi:10.1371/journal.pone.0000717
Philippe, H., Brinkmann, H., Copley, R. R., Moroz, L. L., Nakano, H., Poustka, A. J., Wallberg, A., Peterson, K. J. and Telford, M. J. (2011). Acoelomorph flatworms are deuterostomes related to Xenoturbella. *Nature* **470**, 255-258. doi:10.1038/nature09676
Philippe, H., Poustka, A. J., Chiodin, M., Hoff, K. J., Dessimoz, C., Tomiczek, B., Schiffer, P. H., Müller, S., Domman, D., Horn, M., et al. (2019). Mitigating anticipated effects of systematic errors supports sister-group relationship between xenacoelomorpha and ambulacraria. *Curr. Biol.* **29**, 1818-1826.e6. doi:10.1016/j.cub.2019.04.009
Pimentel, H., Bray, N. L., Puente, S., Melsted, P. and Pachter, L. (2017). Differential analysis of RNA-seq incorporating quantification uncertainty. *Nat. Methods* **14**, 687-690. doi:10.1038/nmeth.4324
Ramachandra, N. B., Gates, R. D., Ladurner, P., Jacobs, D. K. and Hartenstein, V. (2002). Embryonic development in the primitive bilaterian Neochildia fusca: normal morphogenesis and isolation of POU genes Brn-1 and Brn-3. *Dev. Genes Evol.* **212**, 55-69. doi:10.1007/s00427-001-0207-y
Ruiz-Trillo, I. and Paps, J. (2016). Acoelomorpha: earliest branching bilaterians or deuterostomes? *Org. Divers. Evol.* **16**, 391-399. doi:10.1007/s13127-015-0239-1
Ruiz-Trillo, I., Riutort, M. and Littlewood, D. T. (1999). Acoel flatworms: earliest extant bilaterian Metazoans, not members of Platyhelminthes. *Science* **283**, 1919-1923. doi:10.1126/science.283.5409.1919
Ruiz-Trillo, I., Paps, J., Loukota, M., Ribera, C., Jondelius, U., Baguna, J. and Riutort, M. (2002). A phylogenetic analysis of myosin heavy chain type II sequences corroborates that Acoela and Nemertodermatida are basal bilaterians. *Proc. Natl. Acad. Sci. USA* **99**, 11246-11251. doi:10.1073/pnas.172390199
Ruiz-Trillo, I., Riutort, M., Fourcade, H. M., Baguñà, J. and Boore, J. L. (2004). Mitochondrial genome data support the basal position of Acoelomorpha and the polyphyly of the Platyhelminthes. *Mol. Phylogenet. Evol.* **33**, 321-332. doi:10.1016/j.ympev.2004.06.002
Sasai, Y., Lu, B., Steinbeisser, H., Geissert, D., Gont, L. K. and De Robertis, E. M. (1994). Xenopus chordin: a novel dorsalizing factor activated by organizer-specific homeobox genes. *Cell* **79**, 779-790. doi:10.1016/0092-8674(94)90068-X
Semmler, H., Bailly, X. and Wanninger, A. (2008). Myogenesis in the basal bilaterian Symsagittifera roscoffensis (Acoela). *Front. Zool.* **5**, 14. doi:10.1186/1742-9994-5-14
Sempere, L. F., Martinez, P., Cole, C., Baguñà, J. and Peterson, K. J. (2007). Phylogenetic distribution of microRNAs supports the basal position of acoel flatworms and the polyphyly of Platyhelminthes. *Evol. Dev.* **9**, 409-415. doi:10.1111/j.1525-142X.2007.00180.x
Sinigaglia, C., Thiel, D., Hejnol, A., Houliston, E. and Leclère, L. (2018). A safer, urea-based in situ hybridization method improves detection of gene expression in diverse animal species. *Dev. Biol.* **434**, 15-23. doi:10.1016/j.ydbio.2017.11.015
Smith, J. P. S., Teyler, S. and Rieger, R. M. (1986). Is the Turbellaria polyphyletic? *Hydrobiologia* **32**, 13-21. doi:10.1007/978-94-009-4810-5_2
Srivastava, M., Mazza-Curll, K. L., van Wolfswinkel, J. C. and Reddien, P. W. (2014). Whole-body acoel regeneration is controlled by Wnt and Bmp-Admp signaling. *Curr. Biol.* **24**, 1107-1113. doi:10.1016/j.cub.2014.03.042
Technau, U. (2001). Brachyury, the blastopore and the evolution of the mesoderm. *BioEssays* **23**, 788-794. doi:10.1002/bies.1114
Telford, M. J., Lockyer, A. E., Cartwright-Finch, C. and Littlewood, D. T. J. (2003). Combined large and small subunit ribosomal RNA phylogenies support a basal position of the acoelomorph flatworms. *Proc. Biol. Sci R. Soc.* **270**, 1077-1083. doi:10.1098/rspb.2003.2342

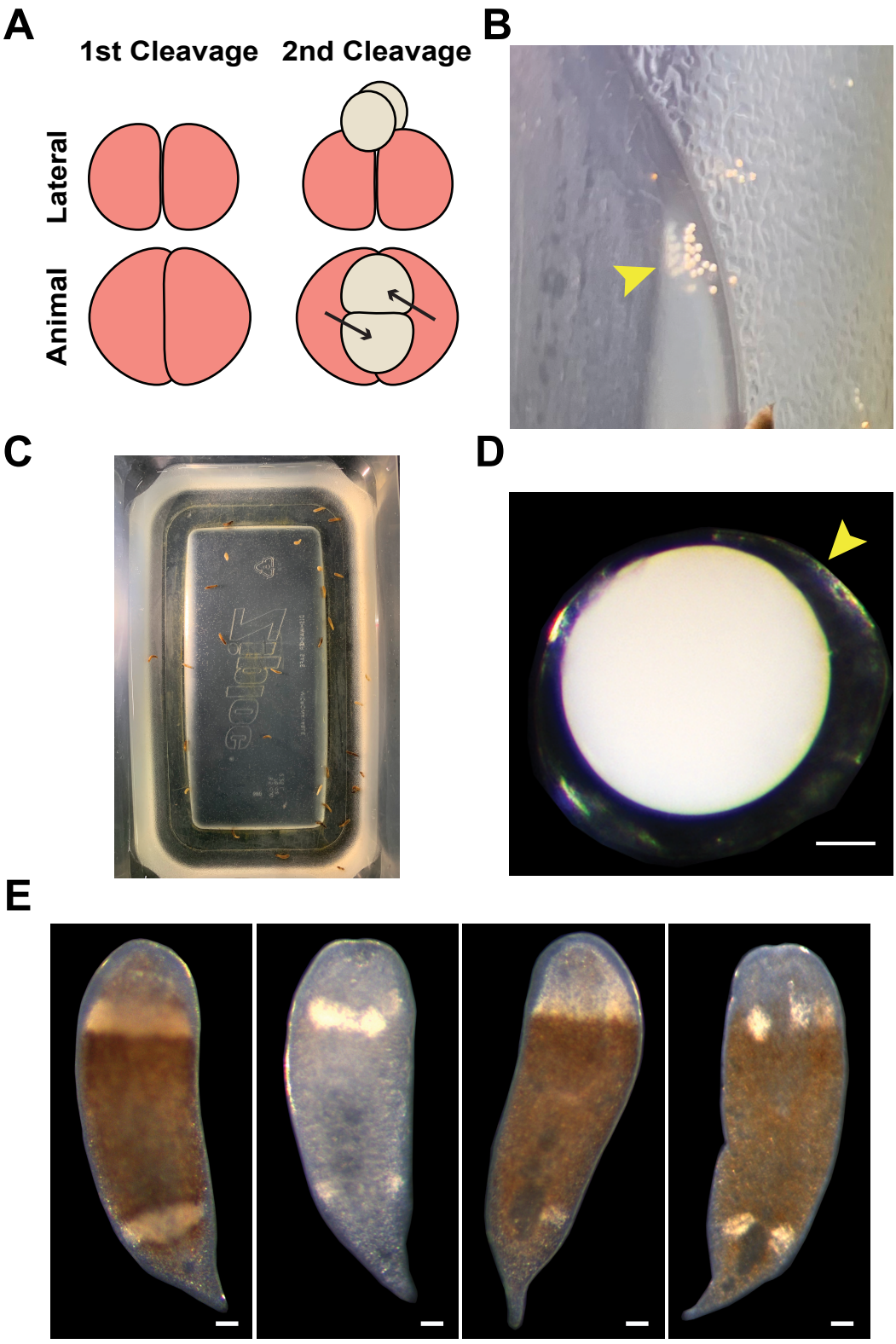

Fig. S1. Culturing *Hofstenia* embryos. (A) Schematic illustrating the first two cleavages of duet cleavage. Arrows denote the counter-clockwise direction of cleavage when viewed from the animal pole. The micromeres (yellow) are situated at the cell junction of the macromeres (red). (B) A representative image of a clutch of *Hofstenia* embryos. (C) Inside of a tupperware box used for culturing *Hofstenia*. (D) Darkfield image of a zygote inside of a clear egg shell (yellow arrow). Scale bar, 100μm. (E) The phenotypic diversity in coloration among *Hofstenia* juveniles.

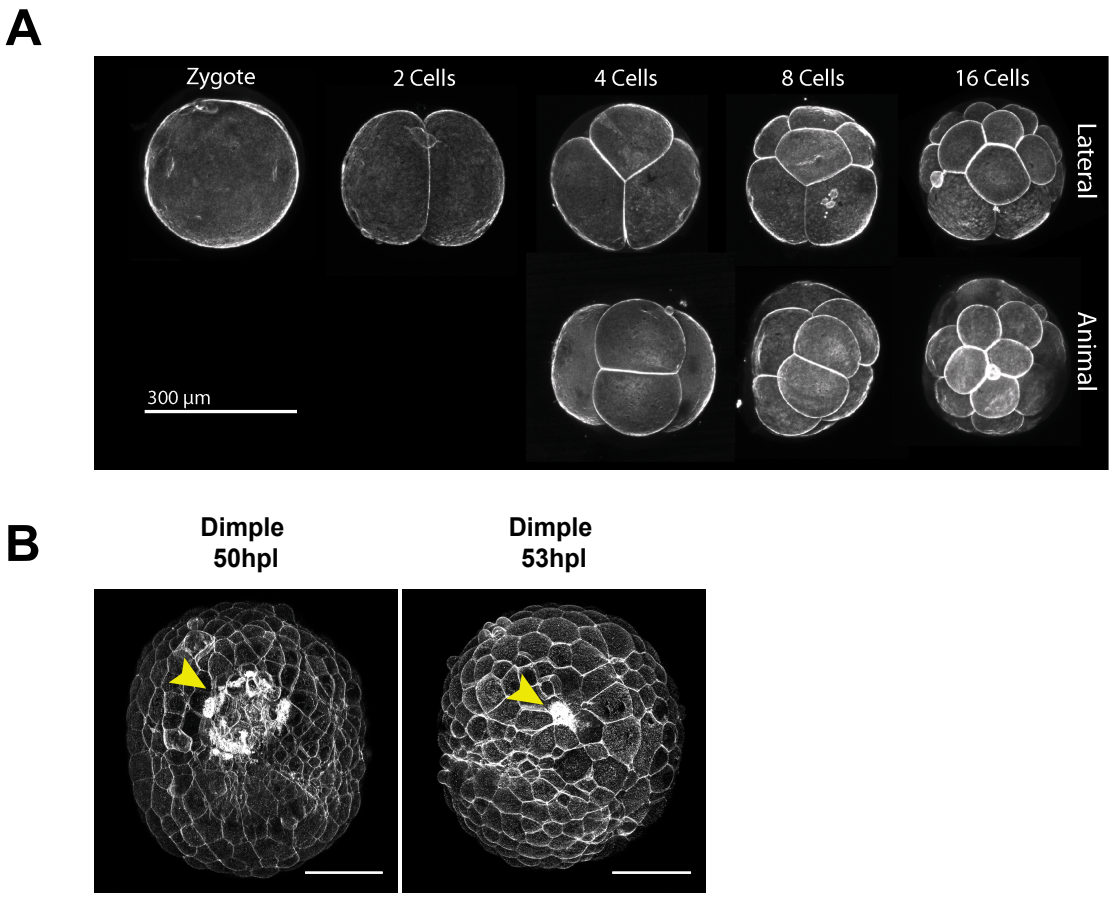

Fig. S2. Phalloidin staining of *Hofstenia* embryos. (A) Representative images of phalloidin stained early cleavage embryos. Scale bar, 300µm (B) Phalloidin stained Dimple stage embryos. A ring of actin is present at the site of cell internalization, or the “dimple”. This ring becomes progressively smaller as the embryo progresses through the Dimple stage. Scale bars, 100µm

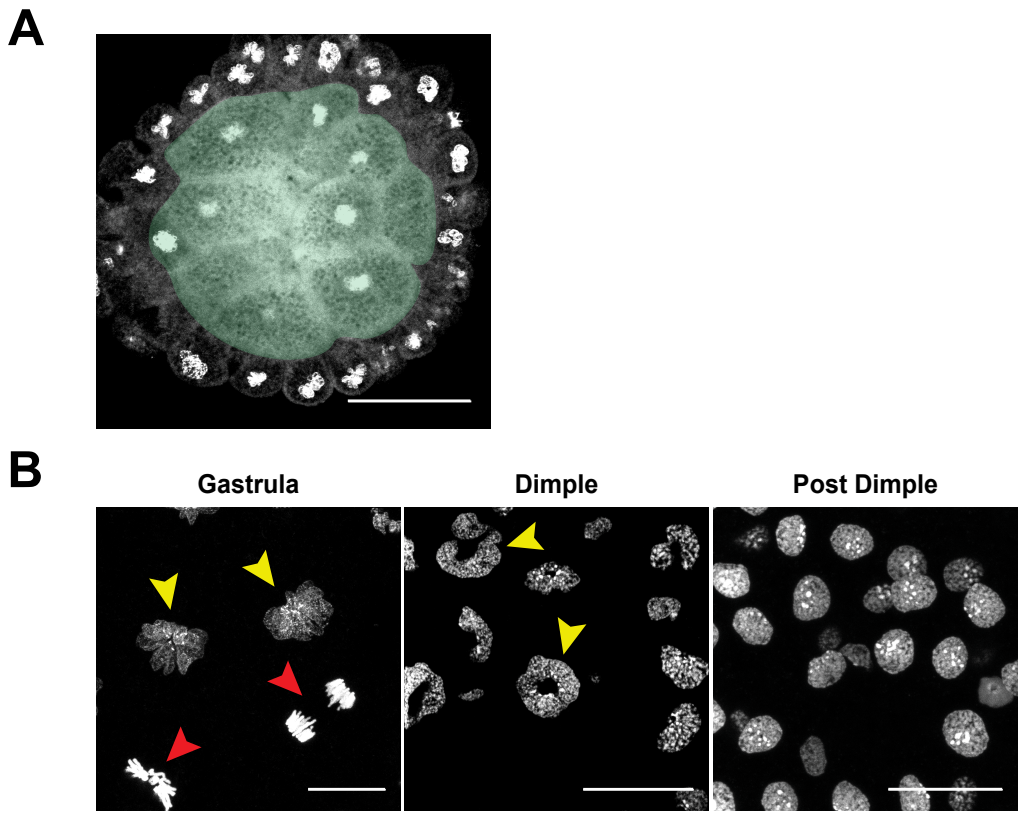

Fig. S3. Nuclear staining of *Hofstenia* embryos. (A) Cross section of a DAPI stained Gastrula stage embryo shows the lack of a blastocoel-like cavity, with the internal space of the embryo being occupied by large cells (shaded green). (B) 63x imaging of Topro3 stained nuclei in Gastrula, Dimple, and Post Dimple stages. A rosette-like shape is present in the majority of Gastrula embryos (yellow arrow), with the exception of cells in anaphase (red arrow). Dimple stage embryos possess ring-shaped nuclei with an empty space at their centers (yellow arrow). Rosette- or ring-shaped nuclei were not detected at the Post Dimple stage. Scale bars, 25μm

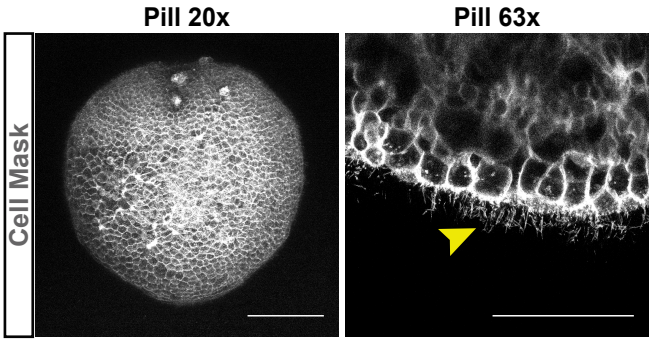

Fig. S4. Cell mask staining reveal the presence of cilia at the Pill stage. Left: 20x magnification image of a Pill stage embryo stained with a Cell Mask plasma membrane dye. Scale bar, 100µm. Right: 63x optical cross section of a stained Pill stage embryo shows the presence of cilia at its surface (yellow arrow). Scale bar, 50µm

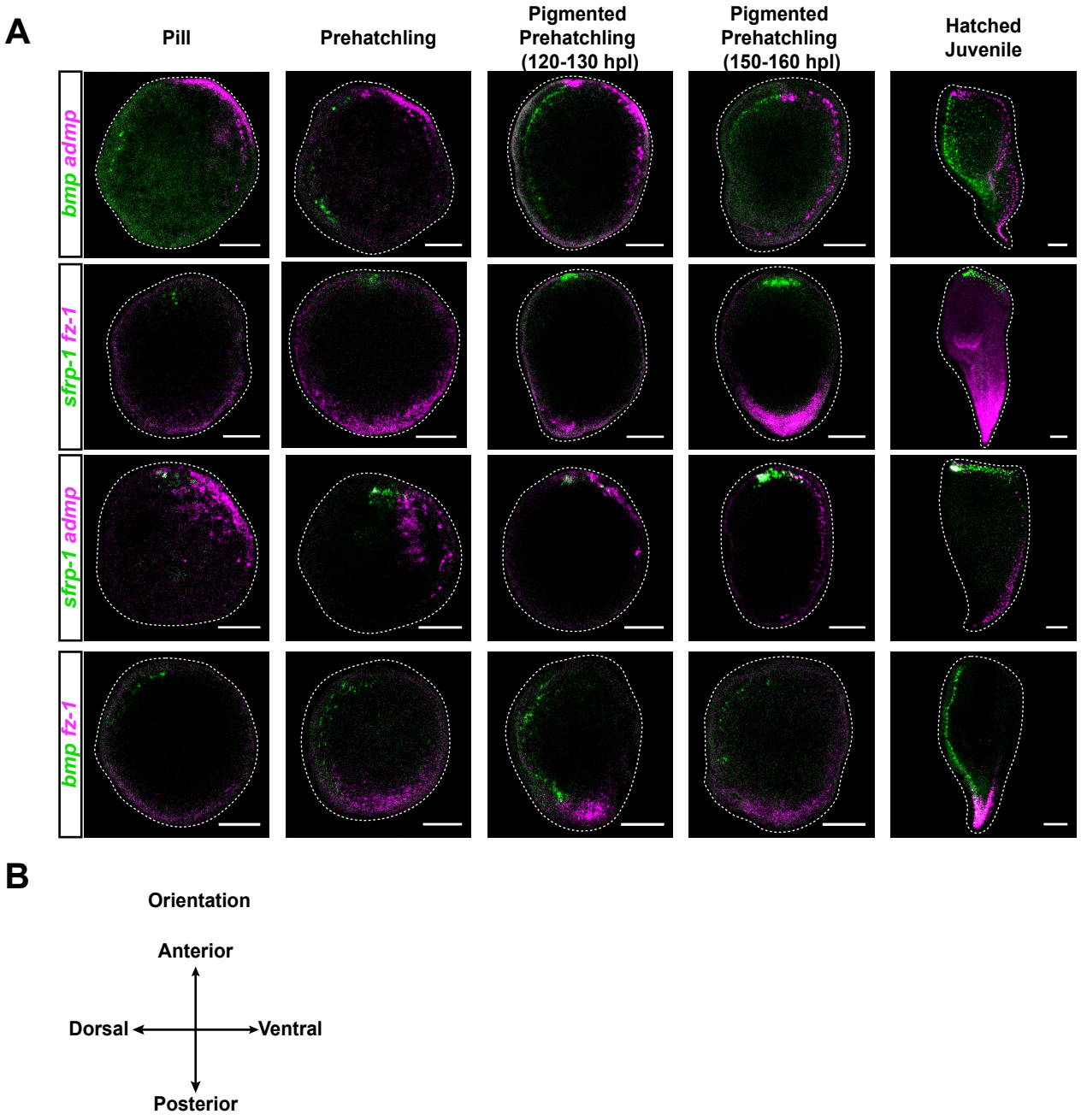

Fig. S5. Expression of axis polarity markers are polarized to opposite poles at the Pill stage. (A) Double *in situ* hybridization of dorsal/ventral and anterior/posterior markers. The dorsal marker *bmp* and ventral marker *admp* occupy opposite regions of the embryo starting at the Pill stage. The anterior marker *sfrp-1* and posterior marker *fz-1* also mark regions that are opposite to each other at the Pill stage. The correct spatial relationship of these axis markers were detected at the Pill stage. (B) Orientation of the embryos shown above. Scale bars, 100μm

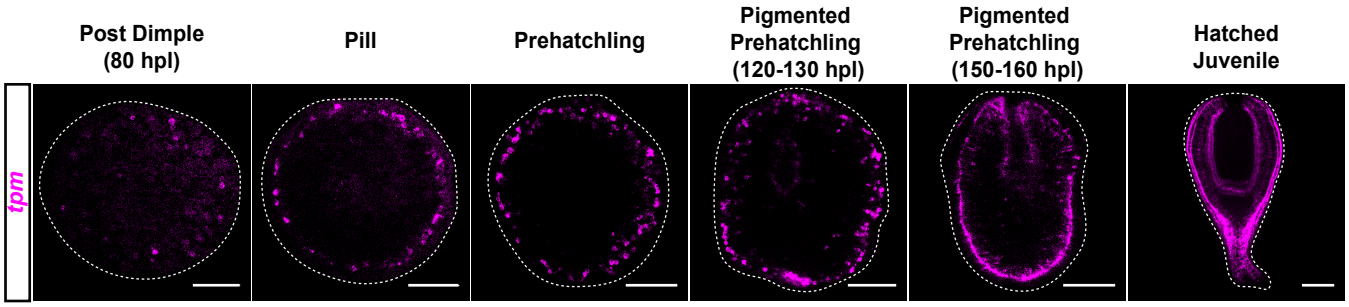

Fig. S6. Cross sections of embryos showing *tropomyosin* expression *in situ*. Optical cross sections of *tpm in situ* hybridizations. Cells expressing *tpm* are situated below the surface of the embryo, but are distributed around the periphery of the cross section. Scale bars, 100μm

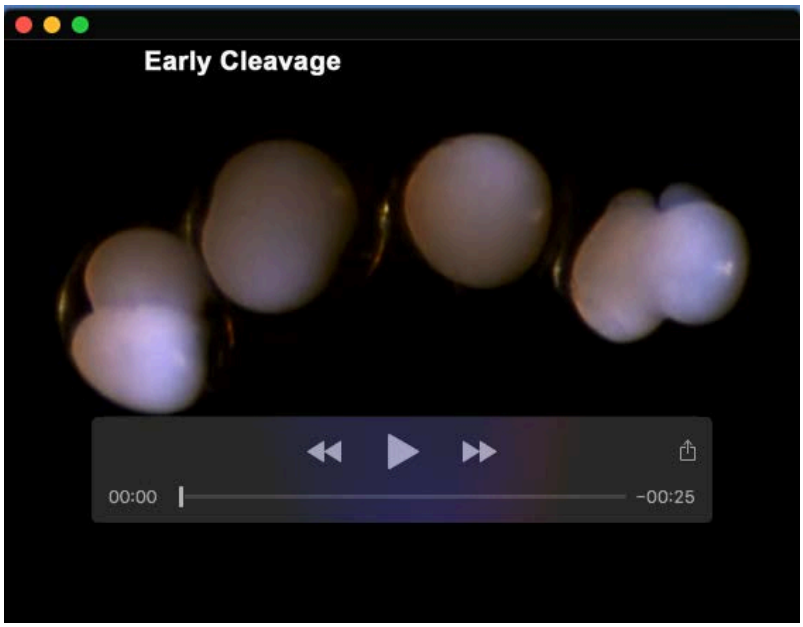

Movie 1. Time-lapse of *Hofstenia* development. Time-lapse recording of one focal plane of embryos from zygote to hatching. This video shows 8 days of development in 2 minutes and 24 seconds. Developmental stages are denoted in the video.

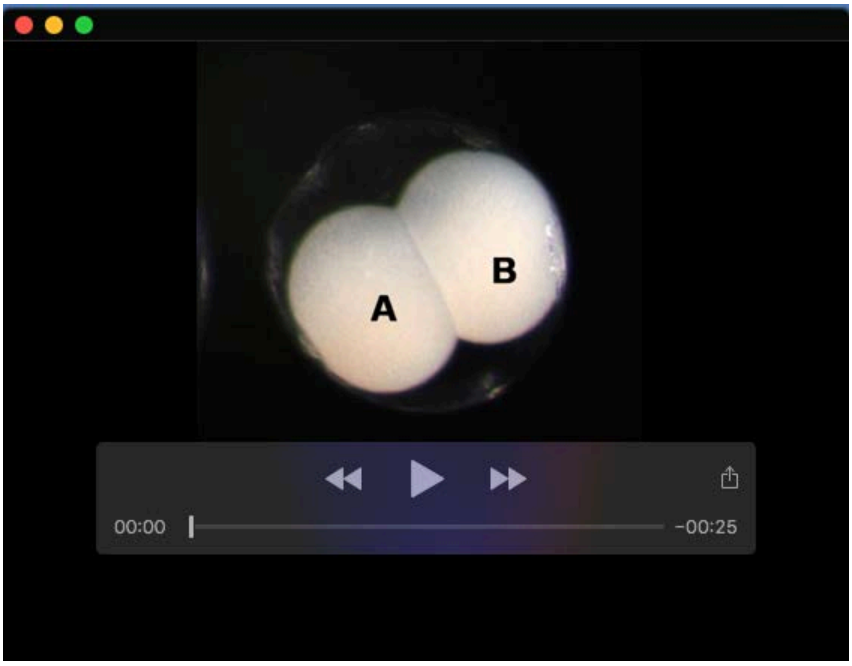

Movie 2. Early cleavage of *Hofstenia*. Time-lapse recording of the first 24 hours of development. The blastomere names that correspond to Fig. 2A are labeled.

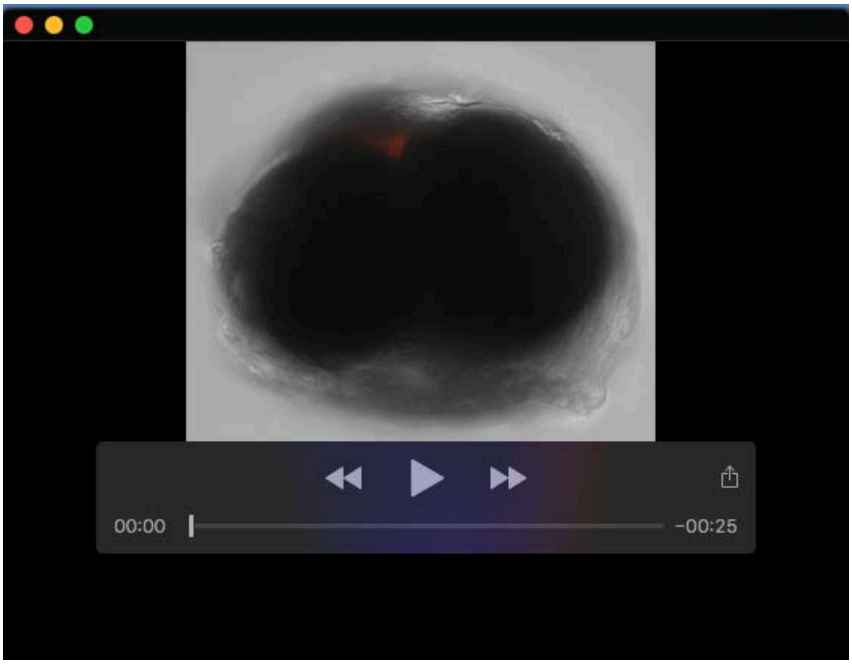

Movie 3. Vegetal view of a *Hofstenia* embryo with 1a and 1b blastomeres labeled with fluorescein dextran. Time-lapse recording of a 4-cell embryo viewed from the vegetal pole after both 1a and 1b micromeres were injected with fluorescein dextran. Labeled daughter cells can be seen moving towards the vegetal pole, internalizing the macromeres in the process.

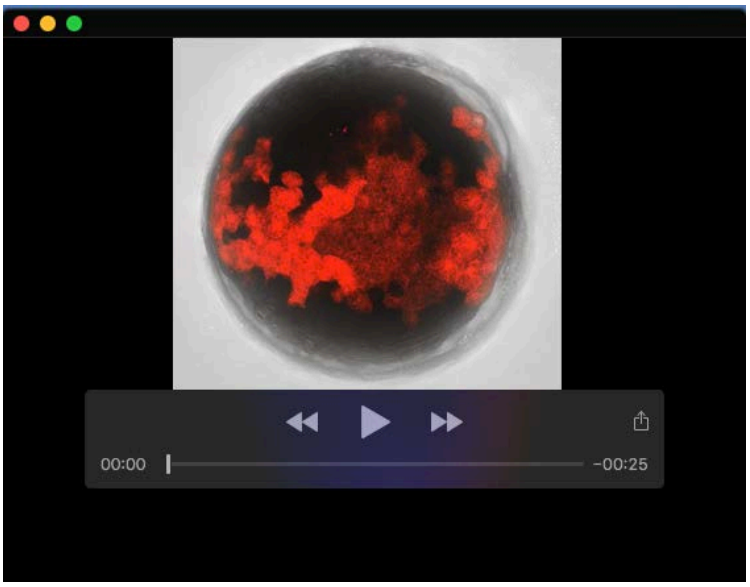

Movie 4. Animal hemisphere view of a Dimple stage *Hofstenia* embryo with 1a and 1b blastomeres labeled with fluorescein dextran. Time-lapse recording of a Dimple stage embryo. All labeled cells are the progeny of the 1a and 1b blastomeres. A patch of labeled cells can be seen being internalized.

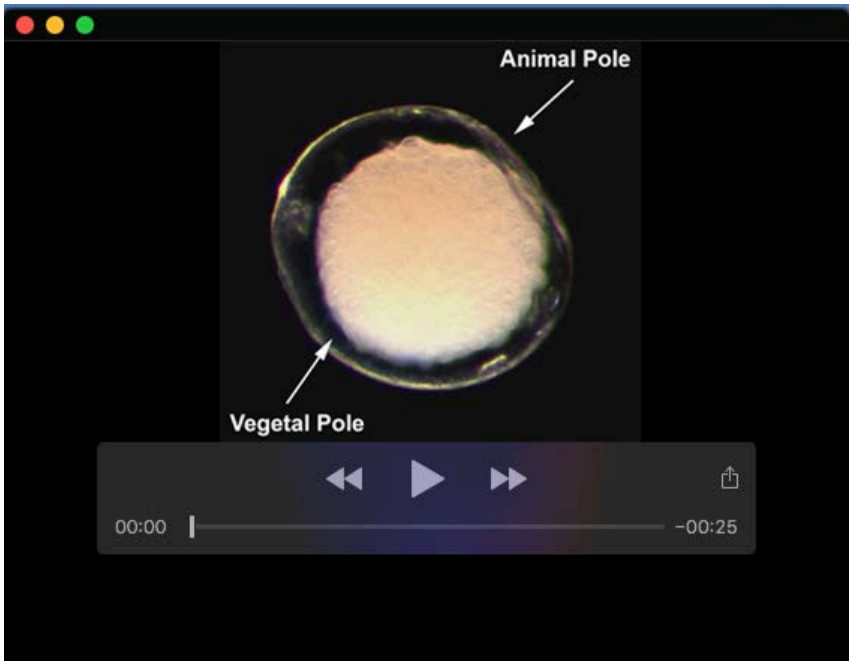

Movie 5. The Dimple stage cell internalization occurs on the animal hemisphere. Timelapse recording of an embryo from a lateral view from the Early Cleavage to the completion of the Dimple stage. The Dimple forms on the animal hemisphere, while the internalization of the macromeres occurs on the vegetal pole.

Table S1. Differentiated cell type marker genes and nomenclature. The justifications for the naming conventions for all previously unpublished genes, sequence and primer sequences.

Click here to download Table S1

Table S2. RNA-seq analysis. (A) GO enrichment analysis results listing the top terms enriched for each cluster along with their multiple comparisons adjusted p-values. (B) Differential expression analysis results showing the adjusted p-values (q-values). (C) Transcripts per million (TPM) values for all genes with at least one statistically significant difference in gene expression across development. This table was used to generate the heatmap in Fig. 5B. (D) Average TPM values for all genes in the *Hofstenia miamia* 70 transcriptome.

Click here to download Table S2